JANUARY 1967

A STUDY TO DETERMINE OPTIMUM LUNAR LIGHTING CONDITIONS FOR VISUAL SELECTION OF LEM TOUCHDOWN POINT

•

FINAL REPORT

•

PREPARED FOR
NATIONAL AERONAUTICS AND SPACE ADMINISTRATION
MANNED SPACECRAFT CENTER
HOUSTON, TEXAS
UNDER CONTRACT NAS 9-5321

Tsun-Ying Feng

PROJECT MANAGER,
T. Y. FENG

HUGHES
HUGHES AIRCRAFT COMPANY
SPACE SYSTEMS DIVISION

SSD 60293R

FOREWORD

This document contains the final report resulting from a ten-month study by Hughes Aircraft Company of Optimum Lunar Lighting Conditions for Visual Selection of the Lunar Excursion Module Touchdown Point. The program was originally contracted as an eight month effort from 12 October 1965 through 12 June 1966 and later extended to 15 August 1966. Concurrent with contract extension one additional task was assigned to Hughes by NASA/MSC. The task was to extend the detection range estimates that include viewing angles of 9 degrees and 55 degrees for sun angles of 5, 10, 15, 30, 45, 60 and 90 degrees and for azimuths of zero and 30 degrees.

At the end of the extended period of the contract, NASA/MSC instructed Hughes Aircraft Co. to withhold publication of the approved final report. The instruction to publish the final report in its original form was received in January of 1967.

The effort described herein was performed by the Space Systems Division of Hughes Aircraft Company as authorized by NASA Manned Spacecraft Center, Houston, Texas, under Contract NAS 9-5321. The Optimum Lunar Lighting Conditions Study is monitored for NASA by Mr. Robert L. Jones of the Lunar Surface Technology Branch, Advanced Spacecraft Technology Division, NASA/MSC and is managed by T. Y. Feng, Hughes Aircraft Company. Mr. Feng's principal assistants are Dr. E. M. Silverstein, who has directed tasks pertaining to the analysis of lunar lighting conditions, and Dr. A. Z. Weisz, responsible for the simulation test, and the human factors evaluation and analysis tasks.

CONTENTS

ILLUSTRATIONS

1. INTRODUCTION

NASA has stated:

> "Prior to an Apollo mission, every effort will be made to select landing areas that afford the greatest possibility of a safe lunar landing. The selection will be based upon current lunar information available at the time for the mission. During the final LEM touchdown maneuver, the command astronaut must visually inspect and evaluate the suitability of the overall area and then select a landing point within the LEM operational range. In order for the astronaut to evaluate a landing area and select the most favorable touchdown point, those parameters influencing site selection must be studied in detail."

Therefore, the purpose of this study as defined by NASA, is to formulate and conduct a program to determine optimum lighting and viewing geometry for the visual evaluation and selection of a landing point within a predetermined landing area.

With this purpose, the objectives of our study can be stated as follows:

1) To determine the detection range of lunar obstacles for a variety of sun elevation angles and viewing geometries.

2) To determine based on visual detectability, optimum and acceptable lighting conditions and viewing geometries during the LEM terminal phase of landing approach for selection of LEM touchdown point, including such effects as LEM vibration, window transmissibility, exhaust plume shimmer, and solar glare.

3) To determine the needs and desirability of the optical aids for improvements of visual evaluation capability in landing site selection.

A work plan to achieve these objectives has been formulated to include the following tasks.

1) Lighting conditions analysis.

2) Human factors evaluation and analysis.

3) Optical aids analysis.

4) Simulation program.

The major effort in this study contract is concentrated on the simulation program because it bears experiment results which will be used to determine the obstacle detection ranges and optimum and acceptable lighting conditions and viewing geometries with critical visual and environmental effects. The simulation program is carried out in an experimental situation in which significant aspects of viewing conditions at a variety of sun elevation and azimuth angles during the LEM's approach, transition, and terminal phase are simulated. The other three tasks, lighting conditions analysis, human factors evaluation and analysis, and optical aids analysis are undertaken in support of the simulation program. The lighting analysis generates the brightness, shadow, and contrast values of lunar obstacles distributed within the LEM landing area for various lighting conditions and viewing geometries. These data coupled with psychophysical considerations, are analyzed for use in obstacle detection range estimates in the human factors evaluation and analysis task. The estimated detection ranges are then compared with those obtained from the simulator tests which, in turn, verify and add precision to the literature-based prediction results. On the basis of the data developed in these tasks, improvements in the visual performance that may be obtained by the use of optical aids have been examined.

The most significant results, attained by this intensified study effort are: (1) the adequacy of the background light resulting from the lunar lighting condition analysis, and (2) the lunar obstacle detection ranges at various sun angles and viewing geometries, from the experimentally-determined predictions in the simulation program and the literature-based predictions in the human factors evaluation and analysis. Combining these two results permits us to recommend the optimum and acceptable lighting conditions and viewing geometries for selection of the LEM touchdown point during the terminal phase of the LEM landing approach.

This report is organized into sections, as summarized below:

1) Section 2, Summary. This section presents a summary

of the important program study findings and recommendations for the optimum and acceptable ranges of the sun angles. Areas for future study not within the scope of the present contract but deemed absolutely essential to the Apollo mission success, are suggested for NASA consideration.

2) Section 3, Lighting Condition Analysis. This section discusses the adequacy of lunar surface background light and presents the obstacle bright side-to-background contrast values and obstacle shadow areas on the homogeneous lunar surface for the analytical obstacle detection range estimate. Discussion on optimum and acceptable sun angles is included. A recommendation of desired lighting conditions and viewing geometries is also offered.

3) Section 4, Human Factors Analysis Technique. This section describes the analytical technique employed to generate the literature-based lunar obstacle detection range estimates. The field factors and Fox edge gradient effects are discussed in predicting the visibility of the lunar obstacles.

4) Section 5, Simulation Program. This section explains in detail, the purpose of the simulation test, obstacle detection model construction, including the obstacle shapes and distribution on the model, and the facilities and light source used in photographing the model. A detailed explanation is given of the technical difficulty encountered in the photographic imagery development. The photographic imagery is the test material for simulation study. Solution to the imagery development problem by means of a new photographic technique is explained in detail. A description of the simulation test equipment and experimental procedures concludes this section.

5) Section 6, Analytical and Experimental Obstacle Detection Range Predictions. This section presents the literature-based and experimentally-derived lunar obstacle detection range predictions. Both results are compared and discussed. Analytical detection ranges with visual and environmental effects such as LEM window transmission loss, light scatter and sun glare are also presented. The last subsection deals with the study results of one additional task stipulated in the contract extension.

6) Section 7, Optical Aid Analysis. This section discusses qualitatively the suitability of an optical aid for visual detection in LEM landing. Advantages and disadvantages of the binocular type optical aid equipment are considered for the lighting conditions at which the LEM landing may be performed.

7) Section 8, Conclusions and Recommendations. Based on the study results reported in the previous sections, conclusions are drawn for optimum and acceptable ranges of sun angles and viewing geometries for visual selection of the LEM landing site. LEM trajectory alteration and optimum search strategy have been discussed. Important work to supplement the present program is recommended.

2. SUMMARY

This section presents, in condensed form, the contract study results by summarizing the significant factual data pertaining to: (1) lighting conditions desired for adequate background brightness, (2) experimentally-determined obstacle detection range predictions as well as those based on literatures, and (3) optimum and acceptable ranges of sun angles and viewing geometries. Recommendations for optical aids and LEM trajectory alteration for visual selection of the LEM landing site are discussed. Finally, a block diagram describes the tasks, summarizes the work performed, and shows results attained during the program. Recommendations for important simulation work to supplement the present program are offered.

2.1 ADEQUACY OF BACKGROUND LIGHTING CONDITIONS

The background luminance for a sun elevation angle as low as 5 degrees, exceeds 50 foot-lamberts for the lunar surface reflectivity of 0.077 for all azimuth angles less than 90 degrees and for viewing angles under approximately 38 degrees. Fifty foot-lamberts is a fairly bright surface, comparable to very good indoor lighting. Therefore, it appears reasonable to state that background luminance is adequate for all viewing conditions being considered when the sun is higher than 5 degrees above the lunar horizon. For sun angles less than 5 degrees, care must be exercised to determine the adequacy of lighting as a background trade-off consideration in determining optimum lighting conditions.

2.2 COMPARISON BETWEEN EXPERIMENTALLY-DETERMINED AND LITERATURE-BASED OBSTACLE DETECTION RANGE PREDICTIONS

The detection range predictions experimentally-determined for the ten-to-one base diameter-to-height ratio, craters and protuberances of Hughes 2 foot height obstacles shown in Figure 5-1, are presented in Figures 2-1 through 2-7 and compared with the analytical detection range predictions based on the data

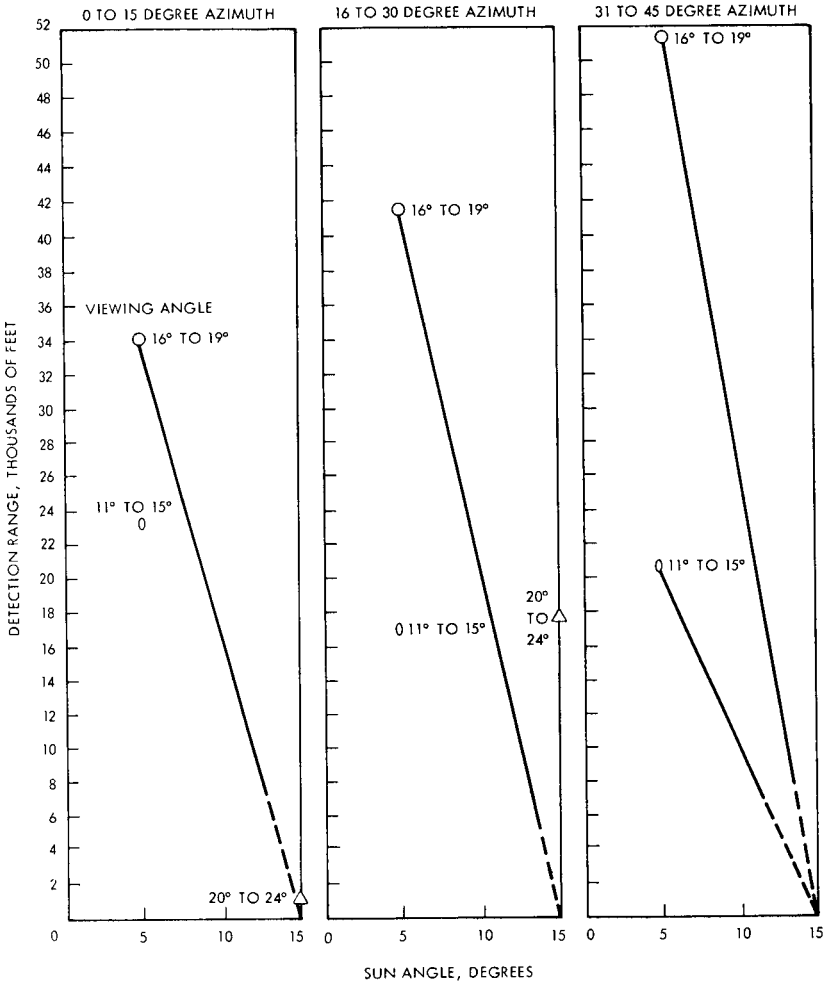

Figure 2-1. Experimentally-Derived Detection Range of Single Spherical Protuberance

gathered by the Tiffany Foundation, with incorporation of the Blackwell field factor correction and Fox edge gradient effects.

The trends of the curves based on two sets of data are in good agreement. The experimentally-determined detection range predictions are approximately twice as large as the literature-based predictions. This is attributed to: (1) the small search area subtended by a small visual angle of 0.8 degrees at the farthest point to 5 degrees at the nearest point in the simulation test, (2) longer search time of approximately 76 seconds, and (3) prior knowledge of the number of targets.

The experimental and analytical results are viewed as bounding the range of visual performance capabilities during the LEM approach, neglecting environmental effects and other adverse factors. The experimentally-determined values apply to visual search of a small, well-defined area such as the immediate vicinity of programmed touchdown point, to which considerable time (on the order of 30 seconds), is devoted for visual search. The more conservative analytical estimates apply to more hurried search of larger areas, where the astronaut is rapidly scanning for an alternate or more favorable landing area.

Several significant conclusions may be derived from these data as follows:

(1) Longer detection ranges are found at low sun angles.

(2) Detection ranges increase with higher (steeper) viewing angles for all sun angles studied.

(3) Viewing angles greater than 25 degrees are necessary to insure moderate obstacle visibility at 0-15° azimuth for sun elevation angles in the vicinity of 15 degrees.

(4) The contribution of azimuth differences between sun and viewing position to the effective phase angle permits a somewhat lower viewing angle of about 20 degrees to be employed with a 15 degree sun while still retaining moderate obstacle visibility.

(5) Detection range differences between protuberance and crater as well as those between single obstructions and clustered groups of four are relatively small as compared to the effects of sun and viewing angle variations.

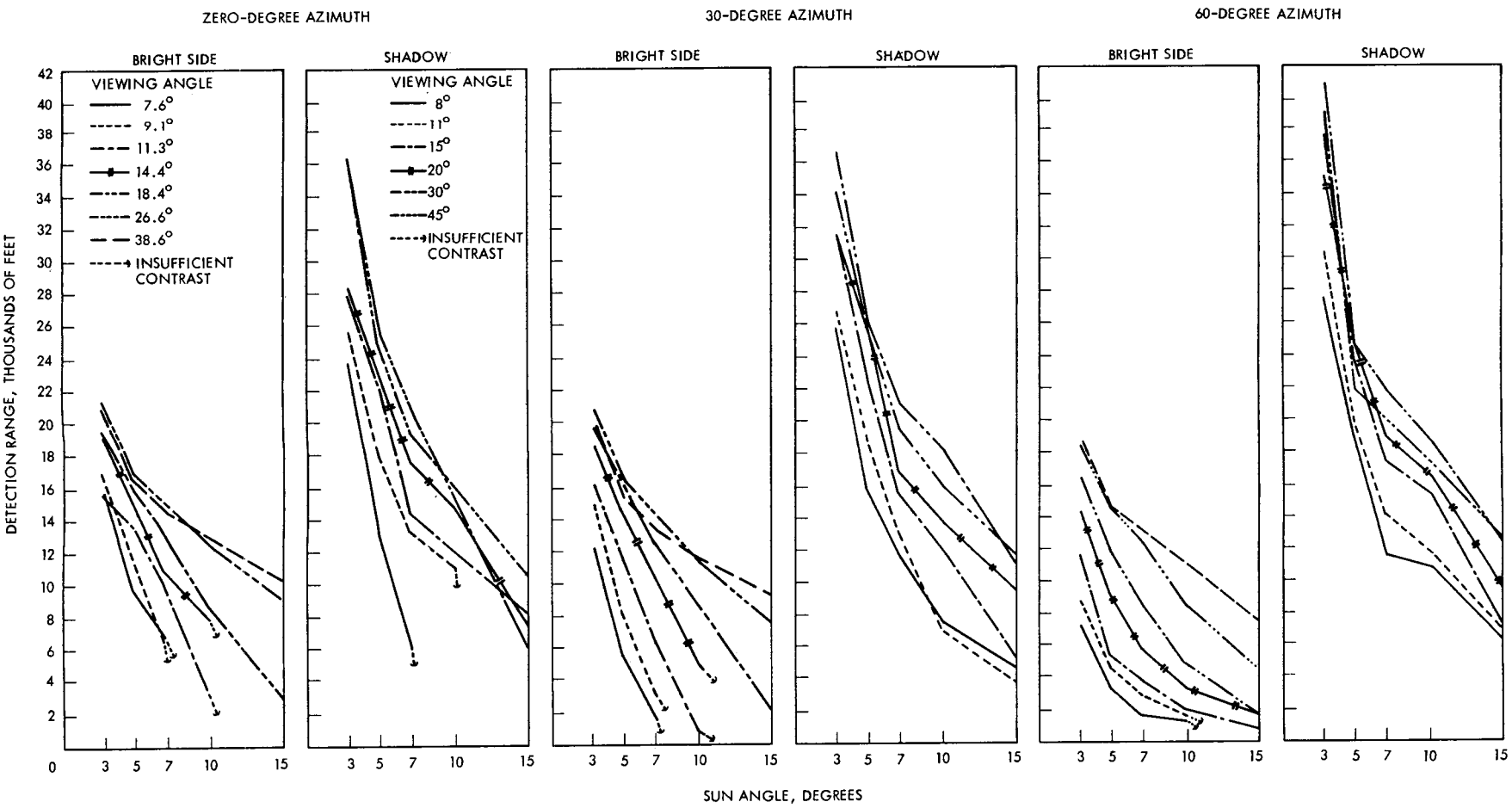

Figure 2-2. Analytical Prediction of Detection Range of Single 8-Sided Protuberance versus Sun Angle for Various Viewing Geometries

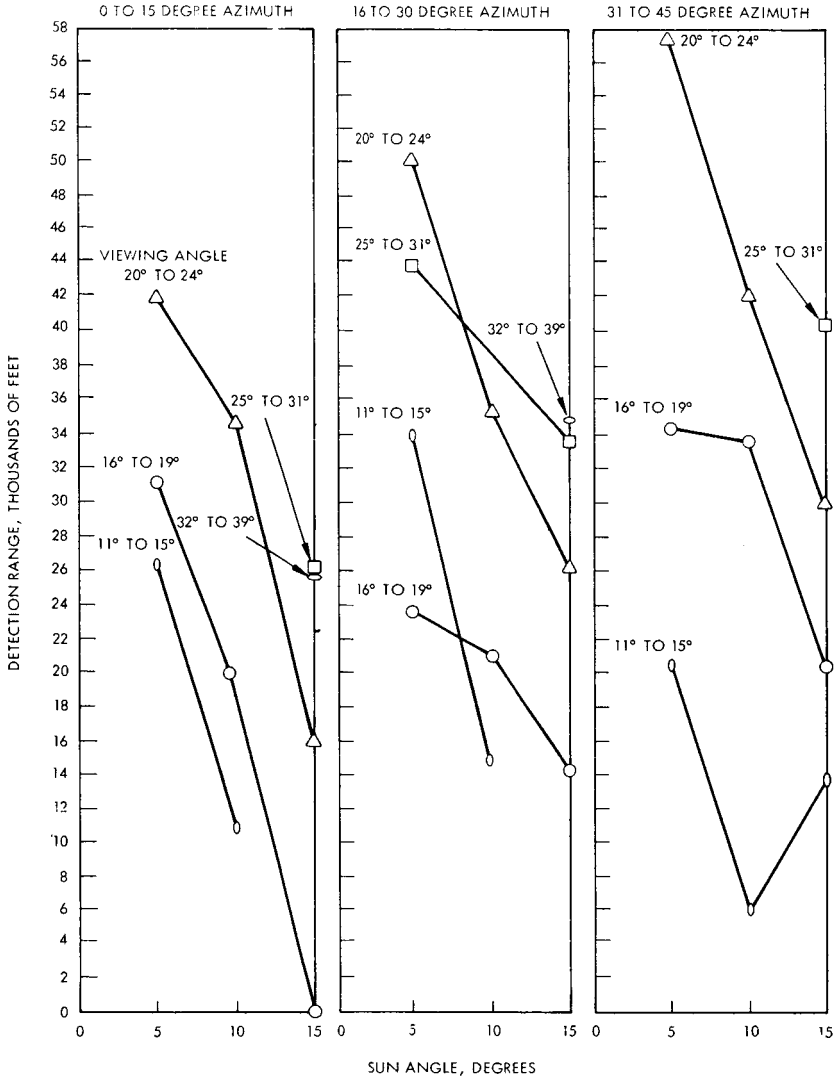

Figure 2-3. Experimentally-Derived Detection Range of Single Spherical Crater versus Sun Angle for Various Viewing Geometries

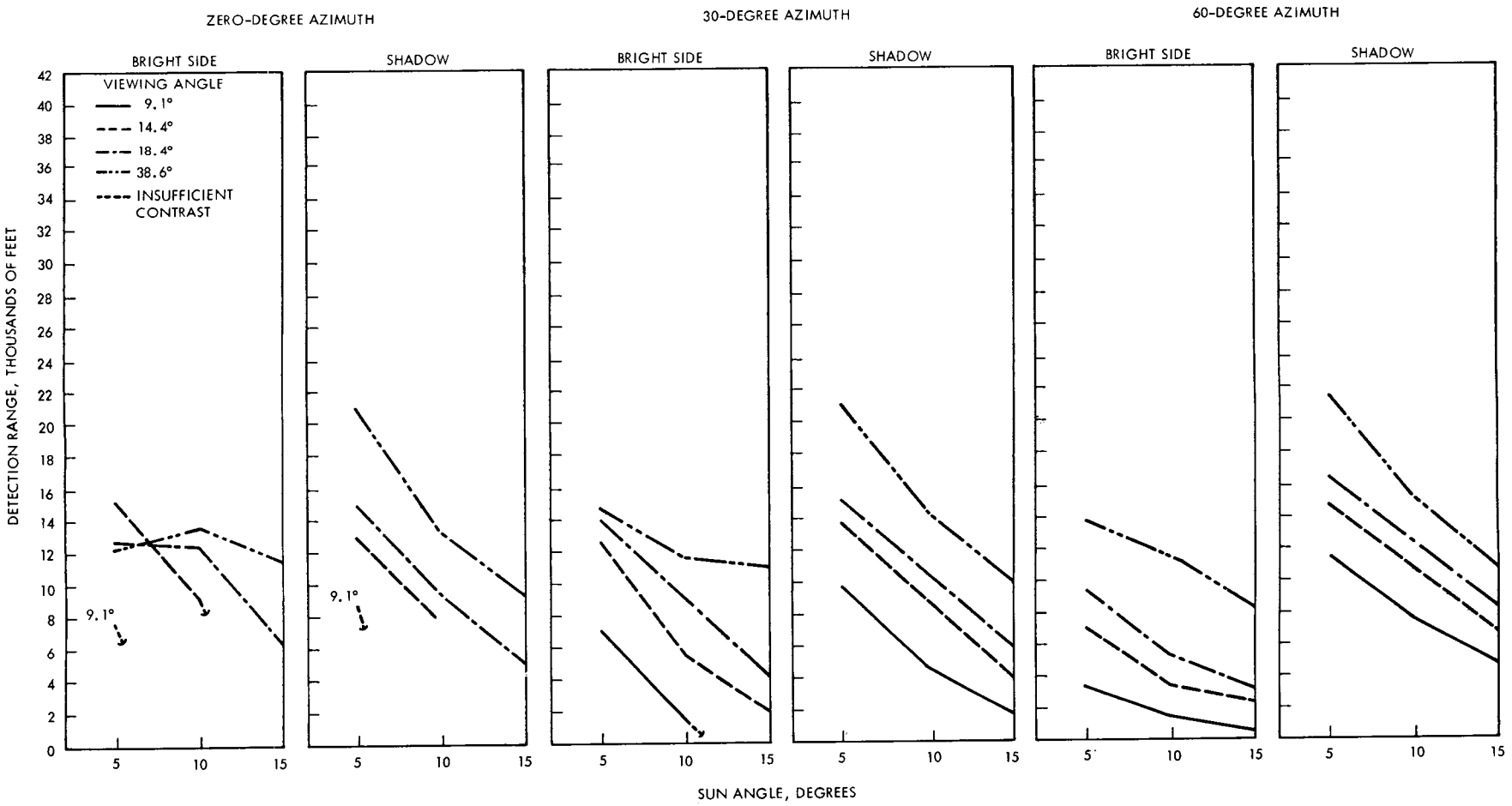

Figure 2-4. Analytical Prediction of Detection Range of Single Spherical Crater verus Sun Angle for Various Viewing Geometries

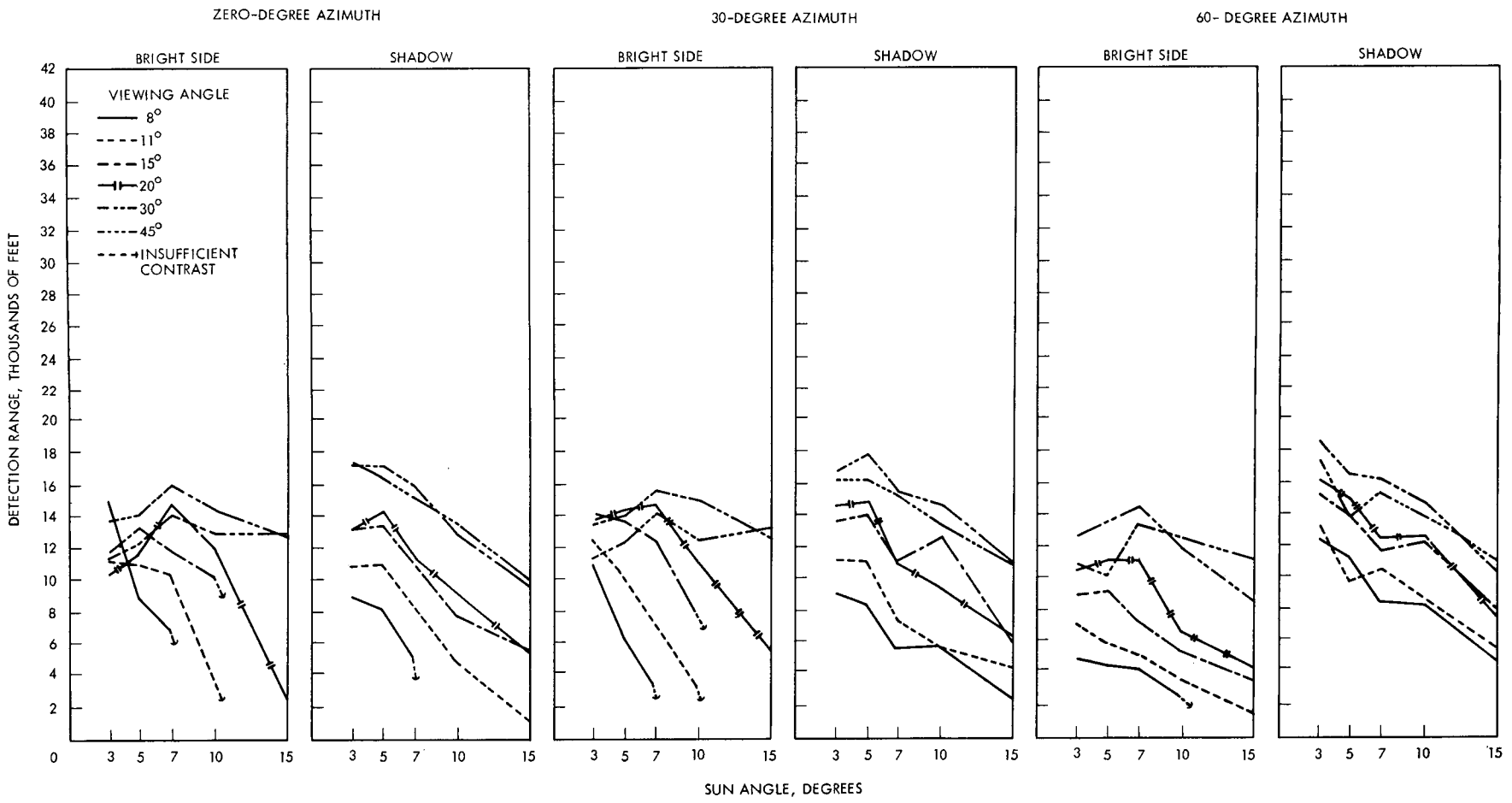

Figure 2-5. Analytical Prediction of Detection Range of Single 8-Sided Crater versus Sun Angle for Various Viewing Geometries

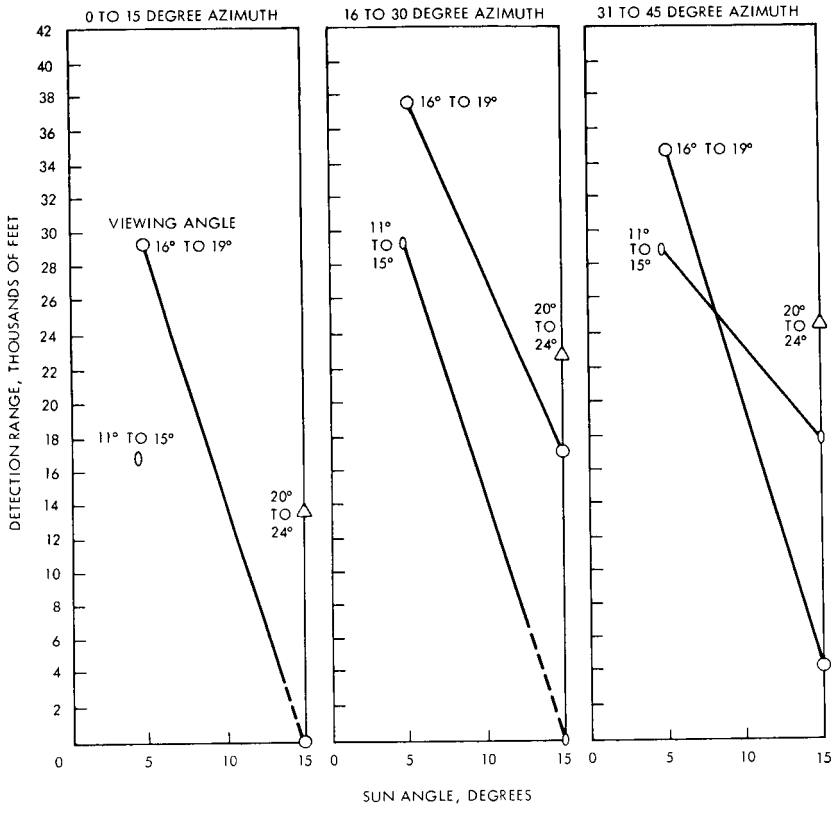

Figure 2-6. Experimentally-Derived Detection Range of Four Protuberances versus Sun Angle for Various Viewing Geometries

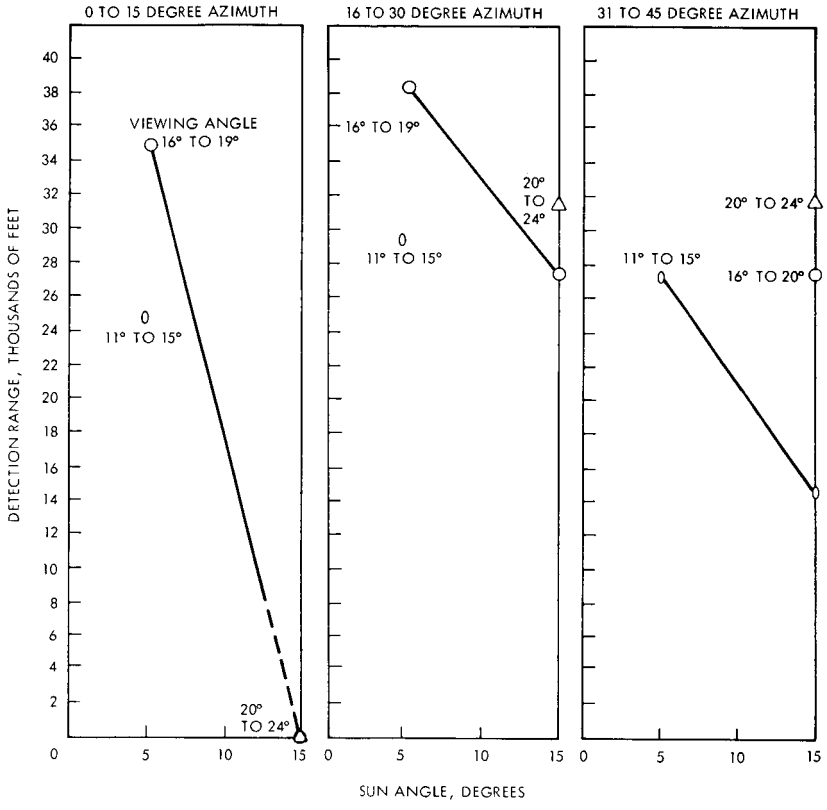

Figure 2-7. Experimentally-Derived Detection Range of Four Craters versus Sun Angle for Various Viewing Geometries

2.3 RECOMMENDATIONS FOR OPTIMUM AND ACCEPTABLE RANGE OF SUN ANGLES AND VIEWING GEOMETRIES, LEM TRAJECTORY ALTERATION AND OPTICAL AIDS

Both the experimental and analytical findings indicate that the optimum sun elevation angles for obstacle detection are between 5 and approximately 8 degrees. Within this range of sun elevation angles, large obstacle shadows combine with excellent bright side-to-background contrast to provide large detection ranges for all viewing and azimuth angles.

The longer detection ranges are obtained with viewing angles higher than the sun elevation angle. Results of this study indicate that these benefits extend to viewing angles up to at least 30 degrees above the sun elevation. This indicates that LEM approach trajectory values of 10-20 degrees are not optimum for landing point selection, particularly when sun angles are above 5 degrees. Therefore, it will be desirable to have LEM trajectory higher than the current maximum value of 20 degrees in order to increase the viewing angles so as to take the advantage of the optimum viewing conditions.

A sun angle of 15^{o} or slightly less should be considered as the highest acceptable sun angle value because at sun angles above 15^{o} all shadow information is lost for the standard obstacles with the gently sloping sides. For sun angles between 15 and 30 degrees, bright side contrast permits some residual obstacle detection capability, but only for viewing angles considerably above the current maximum LEM trajectory angle of 20 degrees. If a sun angle at or near 15 degrees must be employed, higher viewing angles are mandatory, and consideration should be given to the use of a dog-leg maneuver to take advantage of the lower viewing angles permissible with a 30 to 45 degree azimuth. The optical aid analysis indicates that in general the theoretical improvement in detection range, neglecting other factors, to be expected from optical magnification aids is equal to the 2/3 power of the magnification employed. However, the following unfavorable factors will reduce this improvement and minimize the value of optical magnification; (1) the increase in search time required to scan a given terrain area which results from the smaller area which can be scanned in a single visual fixation using the optical aid, (2) the difficulty of carrying out an orderly search of the terrain with a limited field of view, particularly if the astronaut must interrupt visual search for other time-shared activities such as instrument monitoring, (3) orientation problems in relating what is seen by means of the optical aid to the visual scene apparent in unaided vision if distinctive landmarks are not present in the magnified image, and (4) the increased vulnerability to degradation of visual acuity due to vehicle vibration and hand tremor, compounded by the difficulty of locating the exit pupil of the

optical aid close to the eye if the pressure suit visor is worn.

In view of these factors, optical aid is not recommended.

2.4 LUNAR SURFACE MICROSTRUCTURE VERSUS LUNAR SURFACE MACROSTRUCTURE

Preliminary estimates indicate the degradation in visual performance of obstacle detection range due to lunar surface macrostructure is as shown in Figure 2-8. The effects of macrostructure appeared critical to detectability. Obstacle contrast effectiveness is reduced in the macrostructure background as compared to the microstructure background. The degree to which obstacle detectability will be degraded cannot be estimated without conducting experimental tests which are, however, beyond the scope of our present study contract.

2.5 IMPORTANT WORK SUPPLEMENTAL TO THIS PROGRAM IN VISUAL SELECTION OF LEM LANDING SITE

The important areas which require additional simulation work to supplement the results obtained in this program, are as follows: (1) obstacle size estimation, slope detection and estimation in heterogenous background, (2) the effects of the LEM vibration on visual performance, and (3) search, detection and decision time as a function of viewing time available and time sharing requirements for other work load, concerning landing site selection.

2.6 SUMMARY BLOCK DIAGRAM OF TASKS, RESUMES OF ACCOMPLISHED WORK AND STUDY RESULTS OF THE PROGRAM AND RECOMMENDED WORK SUPPLEMENTAL TO THE PROGRAM

Figure 2-9 is a block diagram which summarizes the tasks performed under this contract. A complete resume of work accomplished and the results of the analytical and experimental obstacle detection range predictions are included. Important work areas to supplement the study results of this program are recommended.

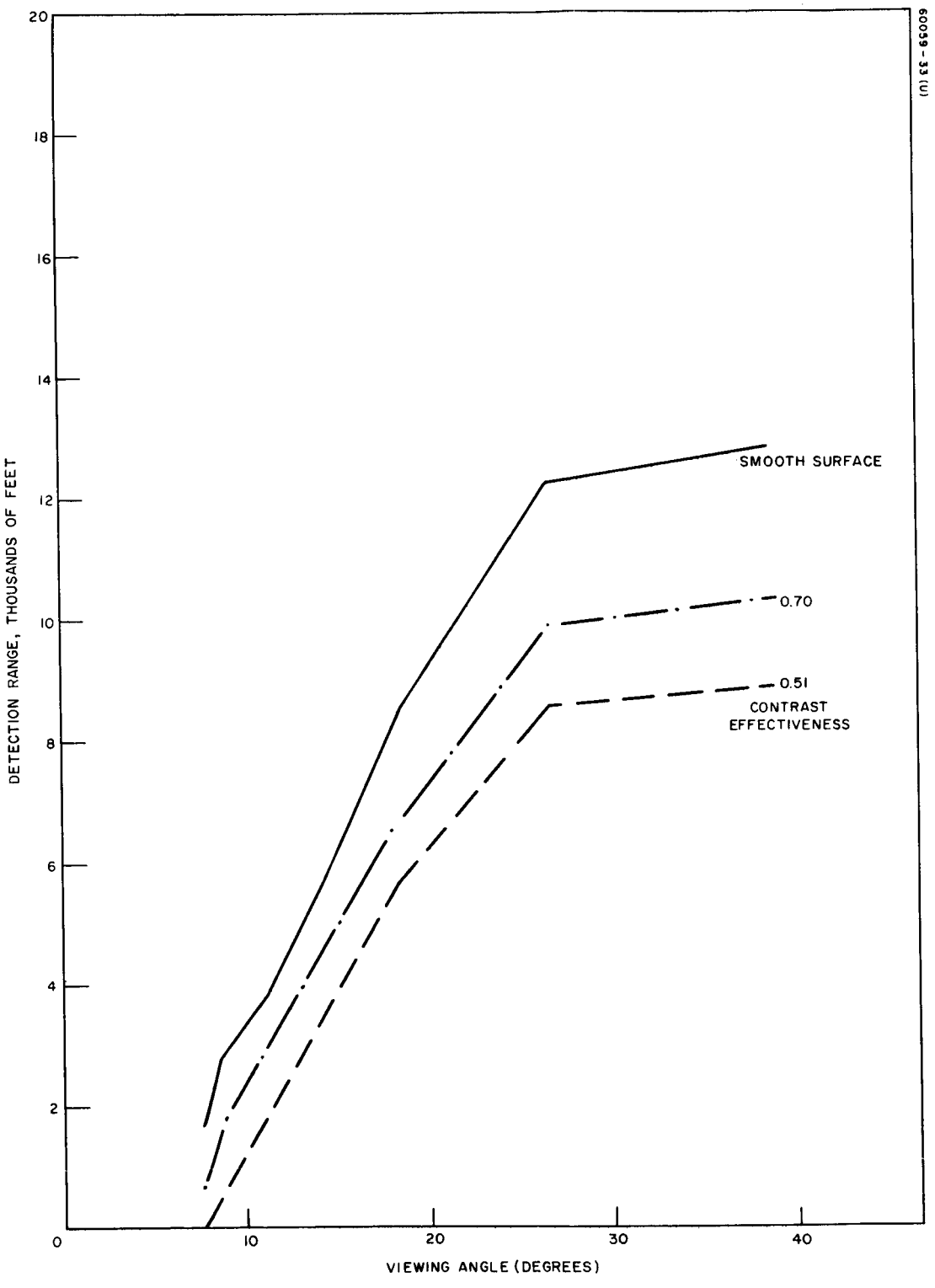

Figure 2-8. Bright Side Detection Range 11.36:1 Cone, 7-Degree Sun Angle, 60-Degree Azimuth – Lunar Surface Macrostructure versus Microstructure

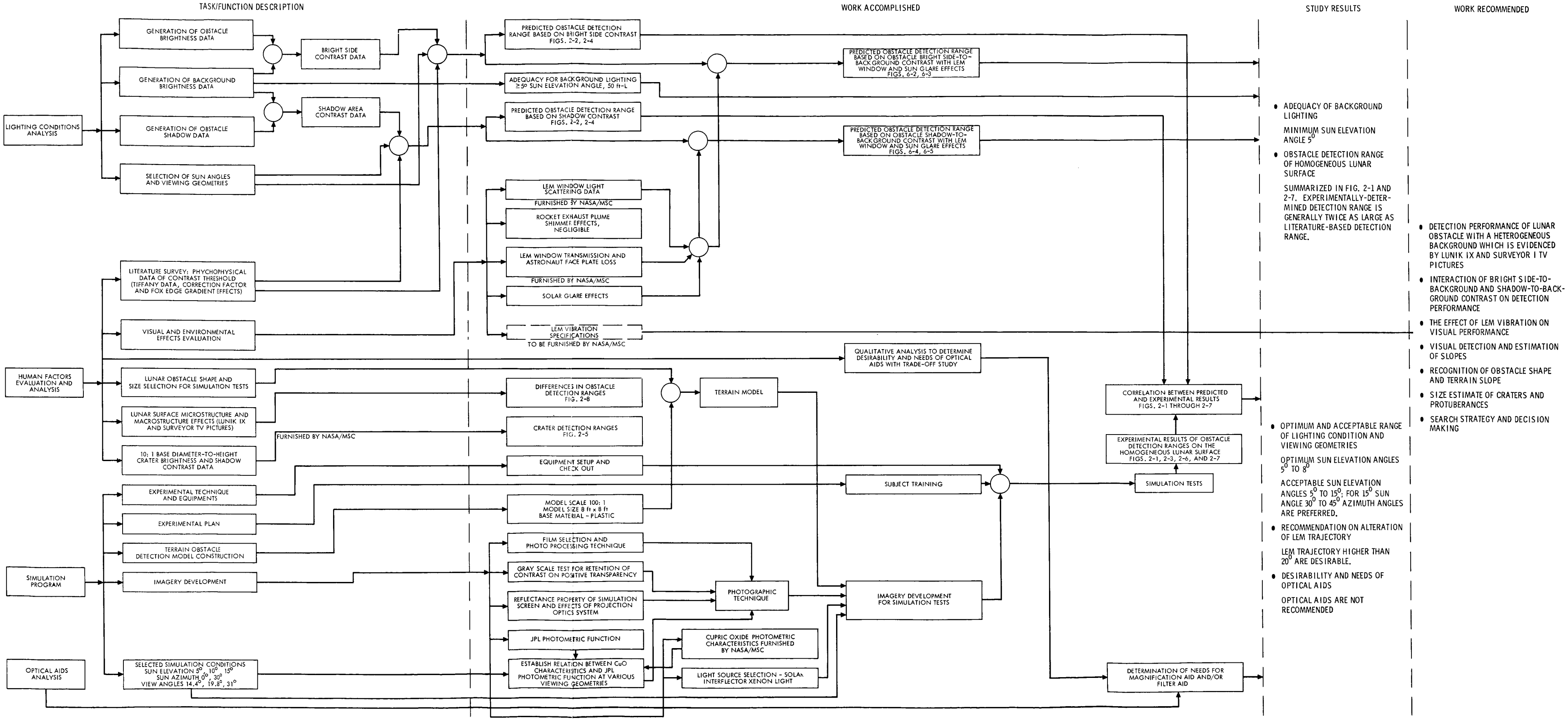

Figure 2-9. Summary Block Diagram of Tasks, Resumes of Work Accomplished and Study Results of the Program and Work Recommended Supplemental to the Program

FOLDOUT FRAME 1

FOLDOUT FRAME 2

FOLDOUT FRAME 3

3. LIGHTING CONDITION ANALYSIS

This section presents the results of the lighting condition analysis; namely,

1) Adequacy of background light, and

2) Obstacle bright side-to-background contrast values and obstacle shadow area on the homogeneous lunar surface for obstacle detection range estimate.

The lunar local surface reflectivity may vary from a low of approximately 0.05 to a high of 0.18. To simplify interpretation of our experimental results, a landing area albedo of 0.077 was assumed. With this albedo, the backbround brightness appeared adequate for all sun azimuth and viewing angles as long as the sun elevation exceeded 5 degrees. Both obstacle bright side-to-background contrast and shadow-to-background contrast suggested very low sun elevation angles for maximum detectability and optimum lighting conditions. The upper limit to an acceptable range of sun elevation angles depends on the specific LEM trajectory and the associated viewing angles, since the contrast values decrease as sun elevation increases. It is always desirable to have sun below the LEM trajectory flight path. The lower limit is strongly dependent on quality of preflight data of local lunar terrain and the detection ranges at the very low sun angles.

The obstacle bright side-to-background contrast values, and obstacle shadow area on the lunar surface are generated for detection range estimate as shown in Section 6, when they are combined together with psychophysical data of contrast threshold.

3.1 ADEQUACY OF BACKGROUND LIGHTING CONDITION

Figure 3-1 is a plot of constant background brightness contours on a lunar map in which the observer is located at a height of 1000 feet at the center of the circles, the sunlight is 5 degrees above the horizon from the 180 degree direction, and

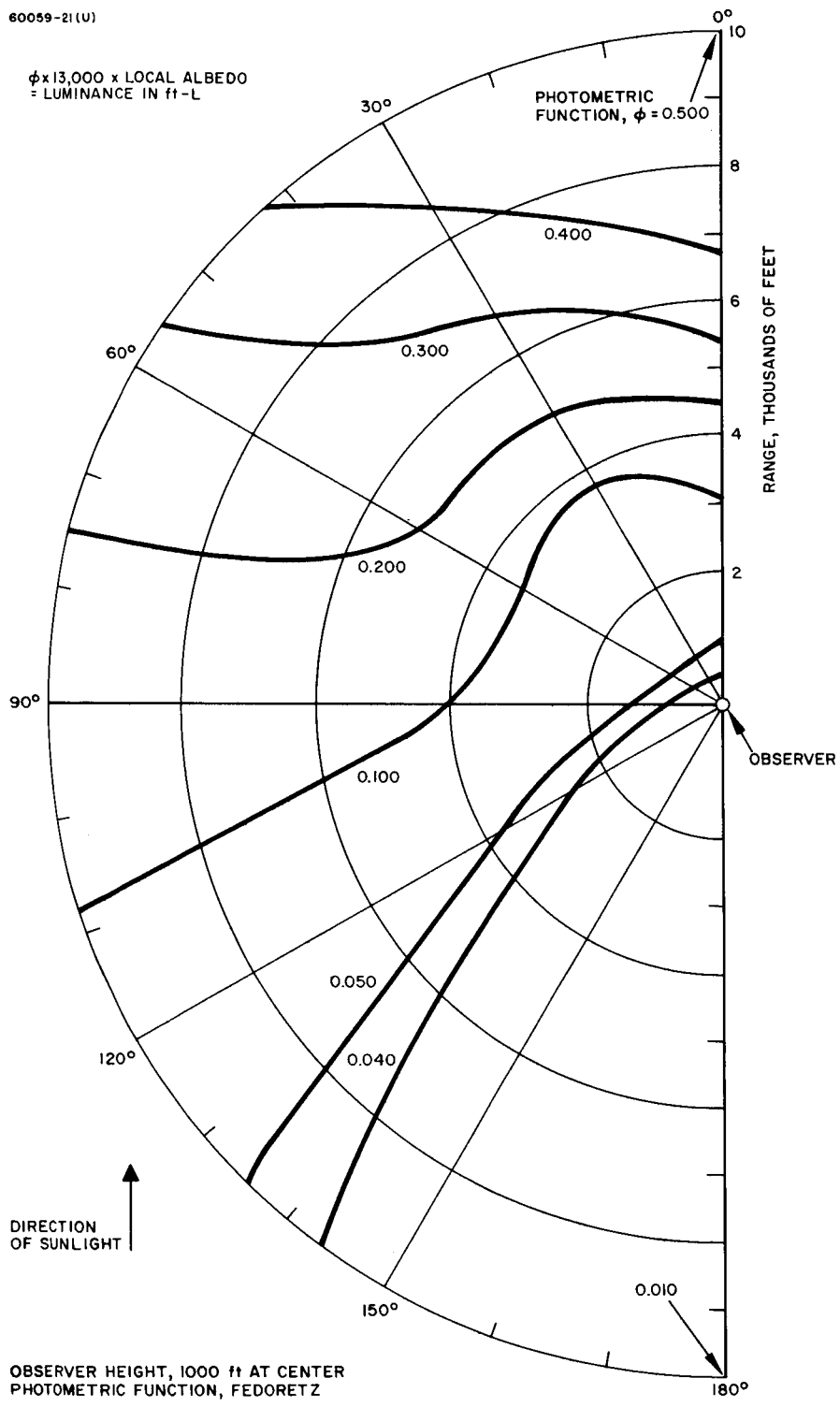

Figure 3-1. Background Brightness Value Expressed in Photometric Function Values Range at 5 Degrees Sun Elevation

radial distances extend out to 10,000 feet as shown. The observer height and radial range may, of course, be scaled together by any amount; the plot is correct so long as the height-to-range ratio (the tangent of the observer's elevation angle) is unchanged. From the figure, it is seen that the background brightness tends to increase with range, and to decrease slowly as the look angle is increased from zero degree azimuth (zero degree azimuth corresponds to the sun being behind the observer). Even for a sun elevation as low as 5 degrees, the background luminance exceeds 50 foot-lamberts (for reflectivity 0.077) for all azimuth angles under 90 degrees and for all observer's elevation angles under about 38 degrees. For most elevation and azimuth angles in the forward semi-circle of Figure 3-1 (the graph is symmetric about the 0 to 180 degrees line), the background luminance is considerably higher than this. As a study of the computer print-outs indicates, the background brightness increases as the sun elevation is increased. Fifty foot-lamberts is a fairly bright surface, comparable to very good indoor lighting, so it would appear reasonable to state that background luminance is adequate for all viewing conditions being considered, when the sun is higher than 5 degrees above the horizon. Even for a sun elevation of 3 degrees, the Fedoretz and the J.P.L. Willingham's data yield luminances exceeding 27 foot-lamberts (for reflectivity $\geq$ 0.077), except for the case of a 45 degree observer elevation and 90 degree azimuth with the J.P.L. photometric function, where a luminance of 19 foot-lamberts is found. Angles below a 3 degree sun elevation give lower background brightness and their adequacy should be examined if these low sun angles are found to be desirable on other grounds. It should be remembered that photometric function values are based on rather poor extrapolated basic photometric data. Therefore, all photometric function values under approximately 0.05 should be used with caution.

In summary, background brightness tends to increase with increasing sun angle when the sun is below the observer and the brightness appears adequate, even for low sun angles as low as 5 degrees. Background light at sun angles lower than 5 degrees is strongly dependent on quality of preflight data of local lunar terrain and visual performance of obstacle detection range.

3.2 OBSTACLE BRIGHT SIDE-TO-BACKGROUND CONTRAST

The contrast values employed throughout this report are derived on the following basis:

$$C = \frac{L_T - L_B}{L_B}$$

where

C = contrast
L_T = target luminance
L_B = background luminance

Contrast is positive if the target area is brighter than the background and negative if the target is less bright. Since negative and positive contrast of equal value give rise to equivalent detectability the direction or sign can be ignored. It has been found in Reference 1 that the brightness contrast is very roughly independent of sun azimuth but is more strongly a function of sun elevation.

The advantages of low sun elevation for highlight detection becomes evident from Figures 3-2 through 3-7. These figures show the bright side-to-background contrast ratio of the Hughes eight sided cone crater (base-to-height ratio of 11.36) as seen by an observer at a 1000 foot elevation, as the sun elevation is varied from 0 to 180 degrees (for the LEM, moving westward at the moon, 0 degrees corresponds to the sun at the eastern horizon, and 180 degrees corresponds to the sun at the western horizon). In each case, the upper curve is for an obstacle at 1000 feet ground range, or a 45 degree elevation angle, and the lower curve is for an obstacle at a ground range of 10,000 feet, or a 5.7 degree elevation angle. Almost all contrast ratios for intermediate ground ranges fall between these two curves. Figures 3-2 through 3-5 are based on the Fedoretz photometric function and have been used to generate the obstacle detection range in Figures 2-2, 2-4 and 2-5 of Section 2. Figure 3-2 is for 0 degree azimuth, Figure 3-3 is for 30 degrees azimuth, Figure 3-4 is for 60 degrees azimuth, and Figure 3-5 is for 90 degrees azimuth. Figures 3-6 and 3-7 are based on the J.P.L. Willingham's photometric function and have been used to generate the obstacle detection range in Figures 6-2 through 6-5 of Section 6.

The main conclusion to be reached from these graphs is that contrast of the bright side of the obstacle against background increases as the sun angle above the horizon decreases; the lower the sun angle, the better, from this point of view. When the sun elevation is higher than that of the observer, the contrast becomes negligible. Considering the low sun angles required before reasonable contrast is obtained with the sun near 180 degrees (in front of the observer) the LEM window light scattering and sun glare effects have made detection impossible (see Section 6-2).

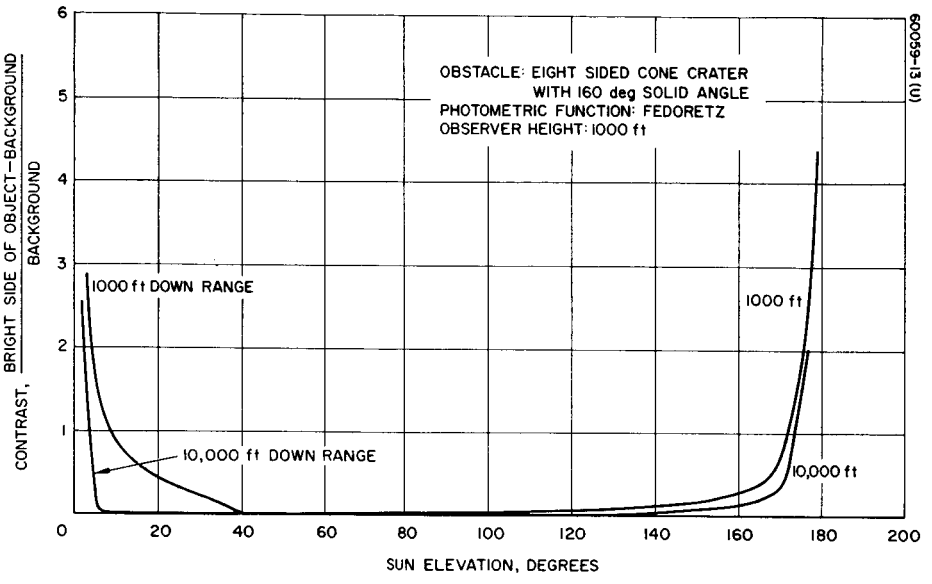

Figure 3-2. Contrast Ratio of Obstacle Bright Side to Background versus Sun Elevation Measured from Local Horizontal at Zero Azimuth Fedoretz Photometric Function

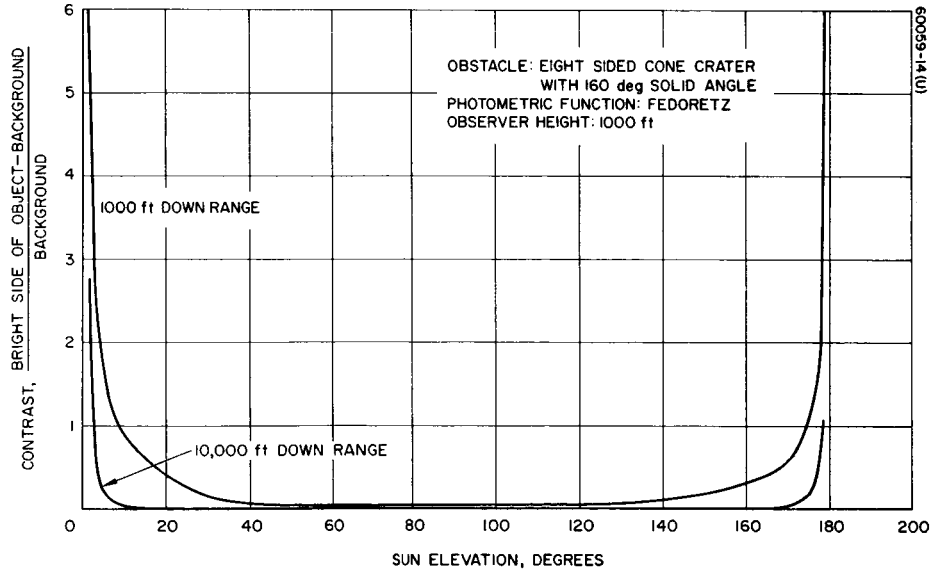

Figure 3-3. Contrast Ratio of Obstacle Bright Side to Background versus Sun Elevation Measured from Local Horizontal at 30 Degrees Azimuth Fedoretz Photometric Function

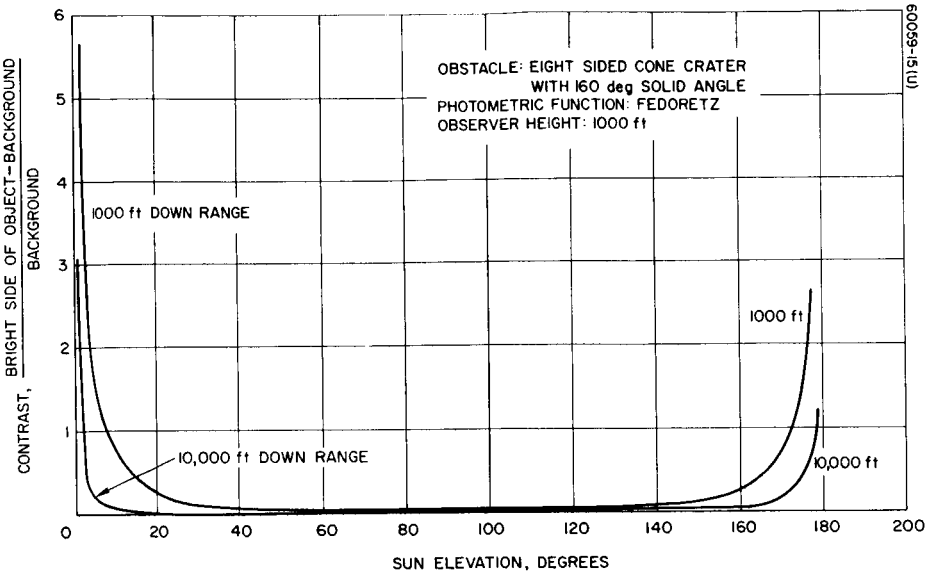

Figure 3-4. Contrast Ratio of Obstacle Bright Side to Background versus Sun Elevation Measured from Local Horizontal at 60 Degrees Azimuth Fedoretz Photometric Function

3-6

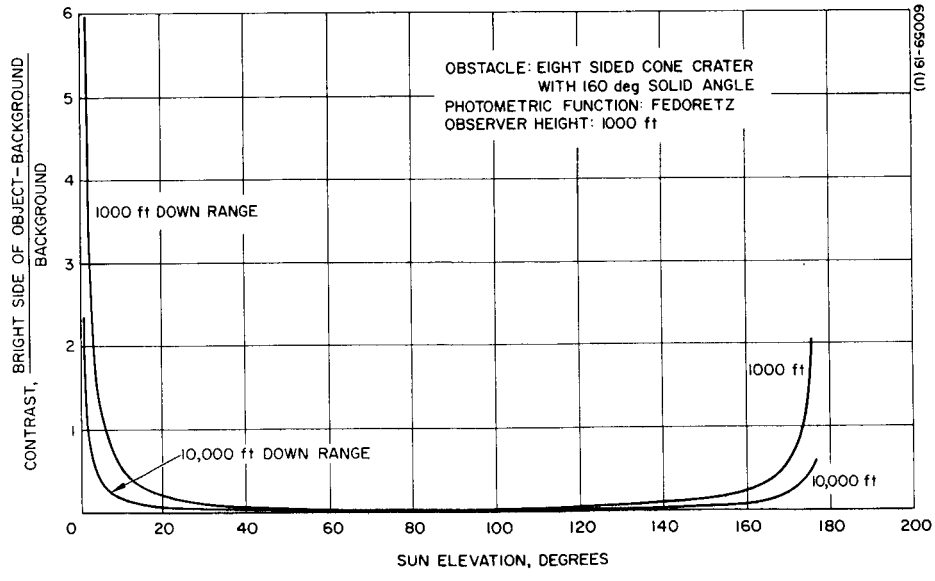

Figure 3-5. Contrast Ratio of Obstacle Bright Side to Background versus Sun Elevation Measured from Local Horizontal at 90 Degrees Azimuth Fedoretz Photometric Function

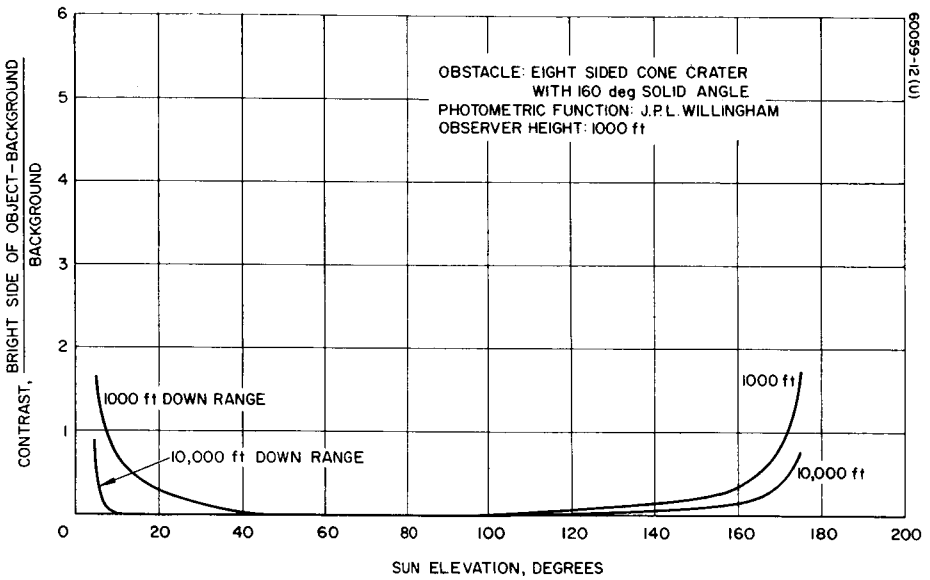

Figure 3-6. Contrast Ratio of Obstacle Bright Side to Background versus Sun Elevation Measured from Local Horizontal at Zero Azimuth JPL Photometric Function

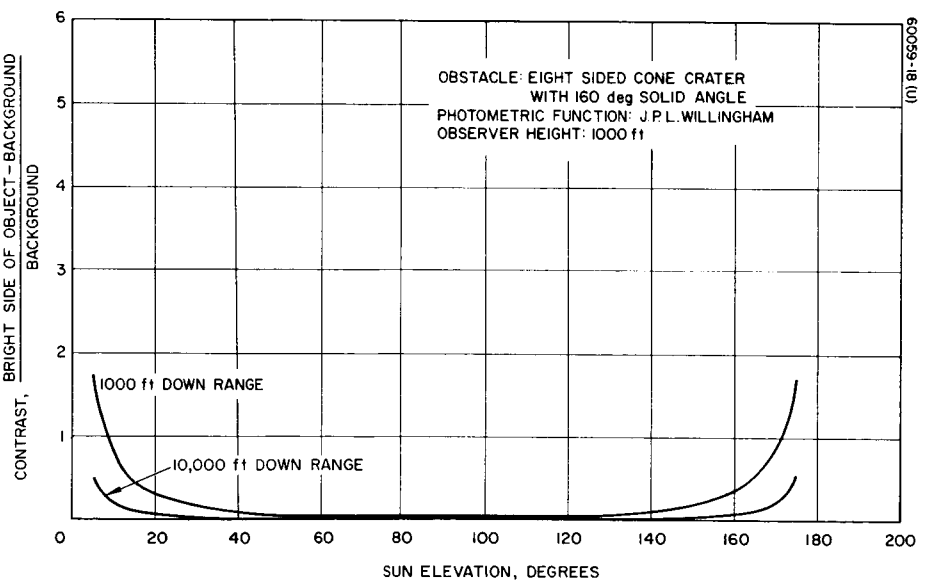

Figure 3-7. Contrast Ratio of Obstacle Bright Side to Background versus Sun Elevation Measured from Local Horizontal at 90 Degrees Azimuth JPL Photometric Function

3.3 OBSTACLE SHADOW AREA

Since the brightness of the obstacle shadow is negligible as compared with that of the background, the obstacle shadow-to-background contrast has been always assumed unity. For low sun elevation angles the presence of a large shadow in or near an obstacle is often its most easily detectable characteristic. An analysis was made, therefore, to determine the shadow size as a function of obstacle shape, and of viewing and lighting geometry. The results are presented in Figures A-1 through A-8 in Appendix A. These figures show normalized shadow area for both convex and concave 10 to 1 base diameter-to-height spherical segment for azimuth angles, 0, 30, 60, and 90 degrees, respectively. On each plot, curves are shown for elevation angles of 8, 11, 15, 20, 30 and 45 degrees. The vertical scales are different for the convex and the concave shapes, since the shadow area for a crater can become no larger than the crater, but the shadow area for a hill can increase without bound.

For the problem of choosing optimum lighting, the chief lesson to be learned from these plots is that the shadow area increases as the sun elevation is decreased. It increases rapidly for the hill, it approaches infinity for 0 degree sun angle, and it increases less rapidly for the crater. Another point of interest is that very high viewing angles allow observance of areas that are relatively independent of azimuth angle; almost all of the shadow is seen from 0 degree azimuth, so nothing much can be gained by a change of azimuth. Lower viewing angles, however, allow observance of increased shadow area as the azimuth angle is increased, both for the crater and for the hill, since a larger part of the shadow is hidden by the obstacle at small azimuth angles.

Thus, we see that the shadows also, as did the bright side contrast, suggest very low sun angles for maximum detectability. The shadow study also suggests viewing distant objects i.e., low viewing angles, from a non-zero azimuth; the farther from zero toward 90 degrees, the larger the visible shadow. However, for look angles near 45 degrees i.e., closer objects, little is to be gained by looking off to the side.

3.4 DISCUSSION ON OPTIMUM AND ACCEPTABLE SUN ANGLES

Thus far, we have determined that both shadow area and bright side-to-background ratio increase as the sun elevation is decreased toward zero. The upper limit to an acceptable range of sun elevations will depend on the specific trajectory in question, and the observer elevation angles required for that trajectory. The lower limit to the sun's elevation, either for the establishment of an optimum condition or of an acceptable range of sun

angles, involves several problems. First, it is strongly dependent on the quality of the preflight data on the local lunar terrain. For example, one could not recommend a 3 degree sun angle if the surface slope were unknown to 5 or 6 degrees. A 5 degree slope away from the sun would cover the entire area in darkness. A 1000 foot range of lunar hills located 8 miles east of the landing site would similarly darken the landing site for a recommended morning 1 degree sun elevation. Considerations such as these will probably set the final lower limit to the recommended optimum sun elevation, and this data may not be available in final form for a specific landing site until shortly before the mission.

Several other considerations could influence the choice of lower sun angle limit, particularly if lunar terrain knowledge is so complete at that time that it sets a minimum of less than 2 or 3 degrees. For one thing, a precise sun angle requires close timing of the mission. A one degree desired sun elevation would still find the sun below the horizon if the landing were attempted 2 hours ahead of schedule.

3.5 RECOMMENDATION

The conclusion based on the lighting condition analysis is that the sun should be in the east (behind the LEM flight path), and the sun angle should be as low as possible, consistent with local terrain information and other mission constraints. For good contrast and shadow conditions, the sun elevation should always be lower than the elevation of the observer. Also, for any given viewing position, the best contrast and the largest shadows are seen when looking down at a steep viewing angle. For a shallow viewing angle from the observer, viewing at a non-zero azimuth angle, perhaps 30 to 60 degrees, gives some improvement in shadow size, but may either increase or decrease bright side contrast, depending on the elevation angles of the sun and the observer.

4. HUMAN FACTORS ANALYSIS TECHNIQUE

4.1 METHOD FOR OBSTACLE DETECTION RANGE ESTIMATION

The lunar surface brightness, contrast, and obstacle projected area data generated by the lighting conditions analysis task have been utilized to estimate the distances at which bright and shadowed areas of standard obstacles are detectable. It was recognized at the outset that the detection range estimates derived from this portion of the program would be subject to error, since the luminance characteristics of lunar obstacles and surroundings differ markedly from the psychophysical test situations in which performance data, on which such estimates are based, were gathered. These analytic predictions of detection were undertaken to examine the relationships between variables as to criticalness and importance for trade-off purposes, to identify the more promising combinations of lighting and viewing angles to be tested in the simulation tests, and to provide preliminary information concerning predicted detection ranges prior to completion of the simulation tests.

The detection range estimates are based upon data gathered at the Tiffany Foundation (Reference 2), relating detection of circular stimuli to target contrast, size, and level of background luminance, as well as on later studies evaluating the effects of various differences between the conditions employed in the laboratory and those normally encountered in everyday use of the eyes. The basis on which field factors have been developed for use in interpreting laboratory data for practical problems, has been summarized by Blackwell (Reference 3). These field factors provide corrections in threshold contrast requirements for the forced-choice test procedure, precise foreknowledge of target location, and 50 percent accuracy criterion employed in the psychophysical test situation, as well as for other psychological differences between laboratory and field conditions. On the basis of this body of work, an increase in threshold contrast of 15 (1.17 log units) appears to be a conservative correction to be applied in utilizing the Tiffany data for the LEM application.

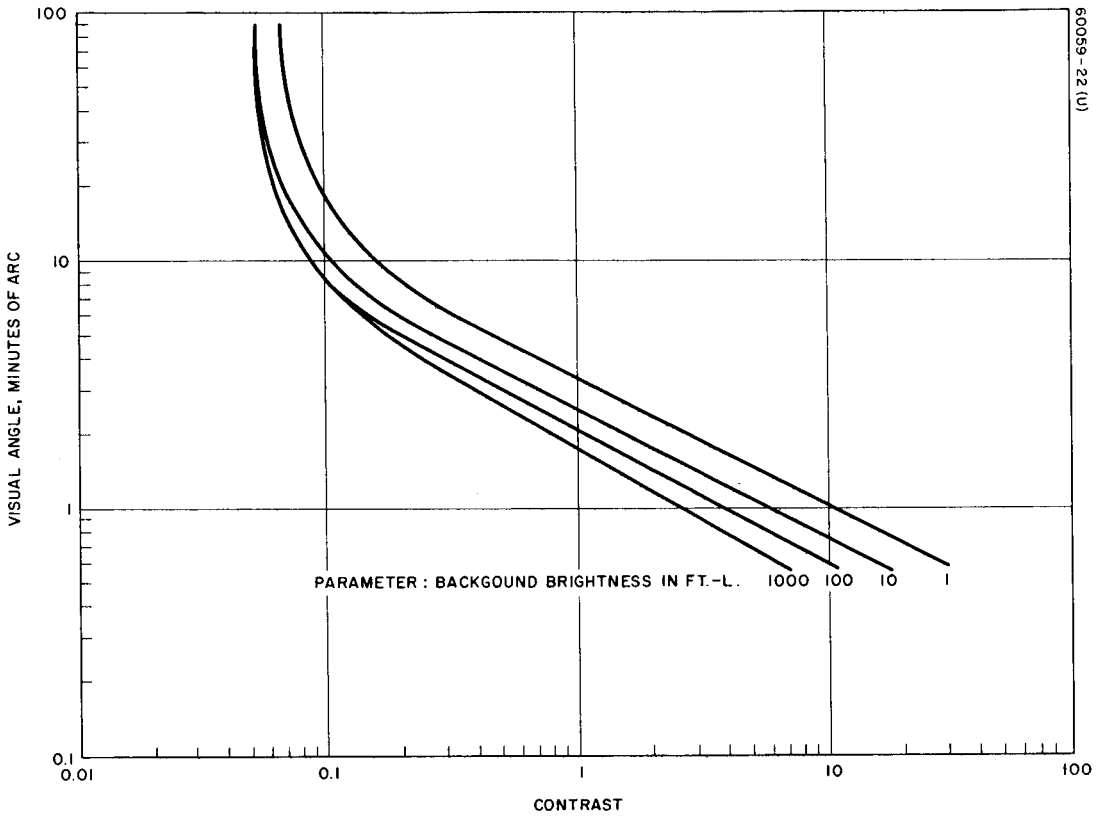

Figure 4-1. Visual Angle versus Contrast for Various Background Brightness Values

A correction factor of 15 has been employed in predicting the visibility of shadow areas associated with lunar obstacles, but a further correction is required for bright-side visibility estimates because of the absence of a sharp contour between bright areas and background. A further increase of 0.1 log units of contrast to correct for edge gradient effects is based upon the results of a study by Fox (Reference 4) concerned with visual discrimination as a function of stimulus size, shape, and edge gradient.

These two correction factors, amounting to an overall increase of 18.6 in threshold contrast, are shown in Figure 4-1 applied to the Tiffany data. The relationships between these basic visual variables of size, contrast, and background brightness, as they apply to the LEM mission, may be seen in Figure 4-1. Background brightness, which lies between 100 and 1000 foot-lamberts for the geometries we have considered, is of minor influence on detection capabilities. For the linear portion of the curves, down to a contrast value of about 0.08, visual size is a more potent determinant than contrast, as evidenced in the slope of the curves. For contrast conditions below 0.08, very large increases in visual size are required to compensate for marginal contrast conditions.

Application of these nomographs to prediction of lunar obstacle visibility presents some difficulties, since standardized lunar cones and craters give rise to areas of varying brightness, such that the brighter areas of the obstacle are characterized by a gradient of luminance ranging from background brightness to some maximum value. The problem is that of selecting the brightness range and associated area to be employed in estimating each bright-side detection range. Kristofferson and O'Connell (Reference 5) have shown that in such situations, adjacent areas of varying contrast contribute to detection according to the squares of the brightness differences between each area and the surrounding background brightness. Thus, areas of small contrast contribute little to effective contrast in the presence of adjacent areas of greater contrast.

The techniques employed to estimate bright-side area and contrast in this study were selected to conform with this finding. In the case of the eight-sided pyramid-shaped obstructions on which Hughes computer-generated data were based, bright-side areas and contrast values were computed from weighted means of the visible areas of the two brightest octant faces. The only exceptions occurred at the largest azimuth viewing angle (60°), where brightest octants were not utilized if the visible area was extremely small. In the case of the spherical crater data supplied to Hughes by NASA-MSC, bright-side area included all parts of the visible surface with brightness equal to or greater than the mean luminance of all

areas brighter than the background, while bright-side luminance was taken as their mean brightness.

A second problem concerned the combining of the negative (shadow) and positive (bright side) contrast values and areas of a lunar obstacle into a single prediction of detection range. At large viewing distances, adjacent negative and positive contrast areas may not be resolved, and thus may cancel one another. At closer ranges, they can be expected to interact to assist in detection. Prediction of these effects for various geometries in which size, brightness gradients, and spatial separation of shadow and bright areas differ, is a complex research problem well beyond the scope of this study. Consequently, independent predictions of positive and negative contrast area detection ranges were computed in order to identify the more promising combinations of lighting and viewing angles for which additional data would be gathered in the simulation test program.

A set of the detection range predictions based on these data are presented in Section 6 together with obstacle detection range estimates derived from the simulation test of this program. The analytical predictions presented in Subsection 6-1 are restricted to sun angles between 5 and 15 degrees, spanning the optimum range of lighting and viewing geometries.

5. SIMULATION PROGRAM

The simulation program is concisered the key to attaining the study objectives of this contract. It is designed to experimentally derive the lunar obstacle detection range estimates which will permit determination of optimum and acceptable lighting and viewing geometries for visual selection of the LEM landing point.

This section presents a summary which includes the purpose of simulation tests, details of the obstacle detection model construction, light source selection for model illumination, photographing of the model, the imagery development, the simulation test equipment, and experimental procedure. A detailed explanation of the technical difficulty encountered in the imagery development effort is included in the imagery development. This is followed by a detailed step by step explanation of the Hughes photographic method developed specially to solve the imagery development problem.

5.1 PURPOSE OF SIMULATION TESTS

The simulation tests, undertaken to verify and add precision to the analytical detection range predictions, were focused on the predicted optimum range of sun and viewing angles. The study was planned to provide more precise absolute predictions of obstacle detection distances within the range of viewing geometries tested, to provide experimental verification concerning the shapes of the curves relating detection capabilities to sun and viewing conditions, and to provide an experimentally determined correction factor applicable to analytical predictions for other viewing conditions.

5.2 OBSTACLE DETECTION MODEL CONSTRUCTION

The terrain models were constructed of a number of plastic modules which contain the lunar standard obstacles. Photographs of the models, after being properly developed, were then utilized in the simulation test. Several materials and construction techniques were investigated for use in model construction. For reasons

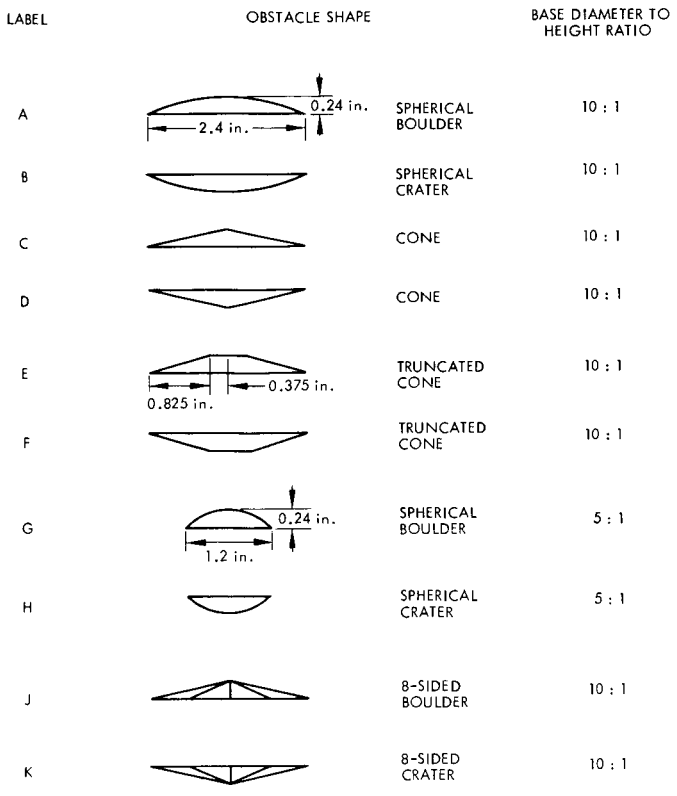

Figure 5-1. Standard Lunar Obstacle for Hughes Simulation Test

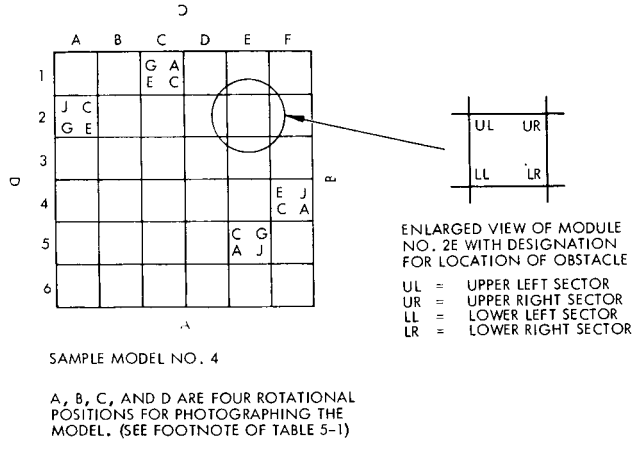

Figure 5-2. Lunar Obstacle Detection Model with Designation of Module Number and Obstacle Location for Nomenclature Employed in Table 5-1 and a Sample Model for Illustration

described below, the plastic material and the vacuum-forming techniques were selected.

Tests with plaster material showed that it was difficult to control the quick setting type so as to form calibrated obstacles. The preparation of a plaster model of a size scaled down to the actual landing footprint area of 8 by 8 feet was found to be an enormous undertaking in the shaping of desired terrain features, thus eliminating the plaster agent for model construction. Attempts to free-form malleable copper sheet showed that craters as large as 2 inches in diameter and one-half inch in height were the maximum sizes which could be produced by hand methods. Requirements for a 0.24 inch size object for the terrain feature in this simulation model were difficult to meet. In addition, control of the geometry of copper shapes was not possible without the proper tooling.

The model size of 8 by 8 feet with a scale factor of 100 to 1 to represent an area of 640,000 square feet, was considered to be large enough to contain the desired numerous combinations of obstacles. The scale factor is dictated by the producible detail of an obstruction of 2 foot height or depth on the lunar model scaled to the largest attainable scale. The obstacle size chosen for the simulation test is based on the "effective protuberances" at the touchdown point specified in Reference 6.

The obstacle shapes and sizes chosen represent 2 foot concave and convex shapes of a truncated cone, regular cone, eight-sided cone, and a spherical section. The spherical section obstacle has both 5 to 1 and 10 to 1 base-diameter-to-height ratio. The other three shapes have a base-diameter-to-height ratio of 10 to 1 (2.4 inches to 0.24 inches). A sketch of the obstacle shapes is shown in Figure 5-1.

The models are assembled from a layout drawing designating the placement of each 16 by 16 inch module. This layout considers the placement of each type of obstacles and the relation of that module to adjacent modules. A mosaic of 36 modules produces an 8 by 8 foot model, representing a lunar area 800 by 800 feet for the 100 to 1 scale. The location of obstacles over the surface of the model are varied in each of the eight models to meet specific simulation test goals. Table 5-1 summarizes the obstacle distribution for various experimental conditions of sun angles and viewing geometries. The method of designating the module number and obstacle location is explained in Figure 5-2. The terrain model was dusted with cupric oxide before being photographed. A typical terrain model is shown in Figure 5-3 prior to CuO_2 dusting. Cupric oxide is dusted on the model by using a Tyler standard screen scale of 325 meshes to the inch, i.e., 0.0017 inch aperture. The sieve and agitator for dusting are mounted on 8 foot parallel bars, with

TABLE 5-1 Lunar Obstacle Detection Model with Obstacle Distributions For Various Experimental Conditions of Sun Angles and Viewing Geometries

Model No.	Module No.	Obstacle Location	Obstacle Shape	Experiment Condition	Sun Angle (Deg.)	Sun Azimuth (Deg.)	View Angle (Deg.)
1	1B	LR	(B)	1	5	0	14.4
	3D	UL	(B)	2	5	0	19.8
	5B	UL	(B)	3	10	0	14.4
	3E	UL	(B)	4	10	0	19.8
2	2A	UR	(B)	5	5	30	14.4
	4B	LR	(B)	6	5	30	19.8
	4E	UL	(B)	7	10	30	14.4
	5F	LL	(B)	8	10	30	19.8
3	2A	UR	(B)	9	15	0	19.8
	4B	UL	(B)	10	15	0	31.0
	1E	LR	(B)	11	15	30	19.8
	5F	LL	(B)	12	15	30	31.0
4	2A	UL(J) UR(C)	LL(G) LR(E)	13	5	0	14.4
	1C	UL(G) UR(A)	LL(E) LR(C)				
	4F	UL(E) UR(J)	LL(C) LR(A)	14	15	0	19.8
	5E	UL(C) UR(G)	LL(A) LR(J)				
5	2A	UL(A) UR(E)	LL(J) LR(G)	15	5	30	14.4
	3F	UL(J) UR(C)	LL(G) LR(E)				
	4C	UL(J) UR(A)	LL(E) LR(C)	16	15	30	19.8
	5D	UL(C) UR(G)	LL(A) LR(J)				
6	3A	UR	(J)	17	5	30	14.4
	1E	LL	(A)				
	4D	LR	(G)	18	15	30	19.8
	5F	UL	(C)				
7	3C	UL	(C)	19	5	0	14.4
	2D	UR	(A)				
	5B	LR	(J)	20	15	0	19.8
	5E	LL	(E)				
8	2A	UL(B) UR(D)	LL(H) LR(F)	21	5	0	14.4
	2F	UL(F) UR(K)	LL(D) LR(B)	22	15	0	19.8
	4C	UL(K) UR(D)	LL(H) LR(F)	23	5	30	14.4
	4E	UL(D) UR(H)	LL(B) LR(K)	24	15	30	19.8

Each of the above eight (8) models is rotated four (4) times for photographing, each rotation is 90 degrees. With the 24 experimental conditions of sun angles and viewing geometries as shown in Table 5-1, 96 imagery pieces are produced for simulation test. The obstacle shapes are shown in Figure 5-1.

the sieve movable laterally to cover all the model sectors as shown in Figure 5-4. After the model is thoroughly covered by the cupric oxide, it is then illuminated by a Xenon light with Hughes solar interflector through two curtain baffles which are used for reducing light reflectance (Figure 5-5). The illuminated model is then ready for photographing (Figure 5-6).

5.3 LIGHT SOURCE SELECTION FOR MODEL ILLUMINATION

The facility selected for photographing the model is located in the Hughes space environment laboratory. This laboratory is equipped with 6000 watt Xenon lamps used in the solar simulator for Surveyor spacecraft simulation tests. The nearly collimated light source well simulates a sun source with approximately one twelfth of solar constant and supplies a beam of uniform intensity suitable for the model photography. The sun source is located in a tunnel area 12 feet wide and 60 feet long, with the walls painted flat black to reduce light reflectance within the area. The model is placed about 60 feet from the light source on a model holding fixture.

The light spectrum generated by the Xenon source of the solar interflector closely approximates the sun spectrum in those frequencies to which the Tri-X-Pan negative film (which has been chosen for imagery development) is sensitive. The light intensity of the source is not critical, since the luminance reflected from the model can be compensated for by controlling camera exposure time so as to produce the same effect as though the model were illuminated by the sun. These corrections are controlled by variations in the film processing.

5.4 PHOTOGRAPHING OF THE MODEL

Photographing of the model was performed in a 60-foot tunnel containing at one end, a Xenon light source whose horizontal beam is centered at 50 inches above the floor, and at the other end a sufficient enlargement of the tunnel width to permit placement of the camera at a 30° azimuth relative to the light. The model was so mounted that its center point rested 50 inches above the floor, and could be tilted about that center to simulate 5°, 10°, and 15° sun angles. Camera positions were then selected to provide (at both 0° azimuth and 30° azimuth) simulated viewing angles of 14.4° and 19.8° for the 5° and 10° sun, and 19.8° and 31° for the 15° sun.

It will be observed that no effort was made to maintain exactly the same distance from lens to model center in these geometries. Subsequent to the photographic process, the precise geometric relationships and actual range values were computed for

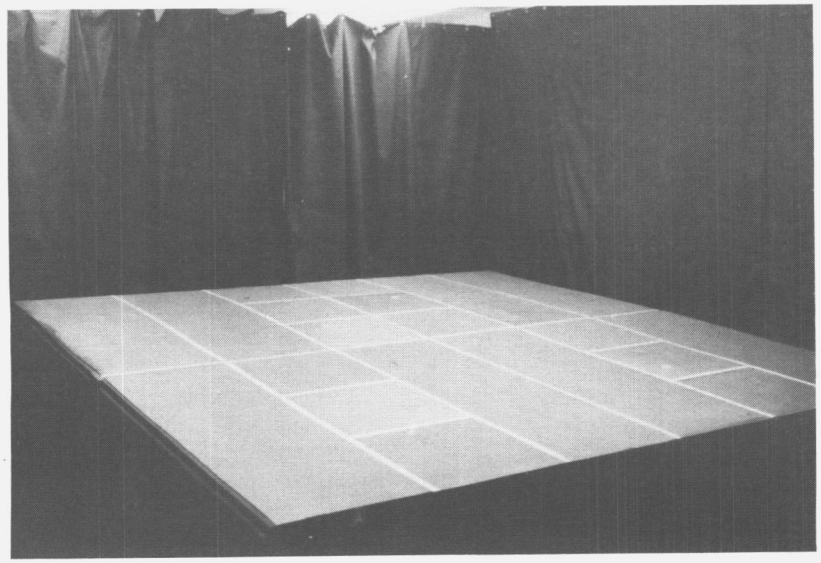

Figure 5-3. Plastic Lunar Model Before Dusting with Cupric Oxide

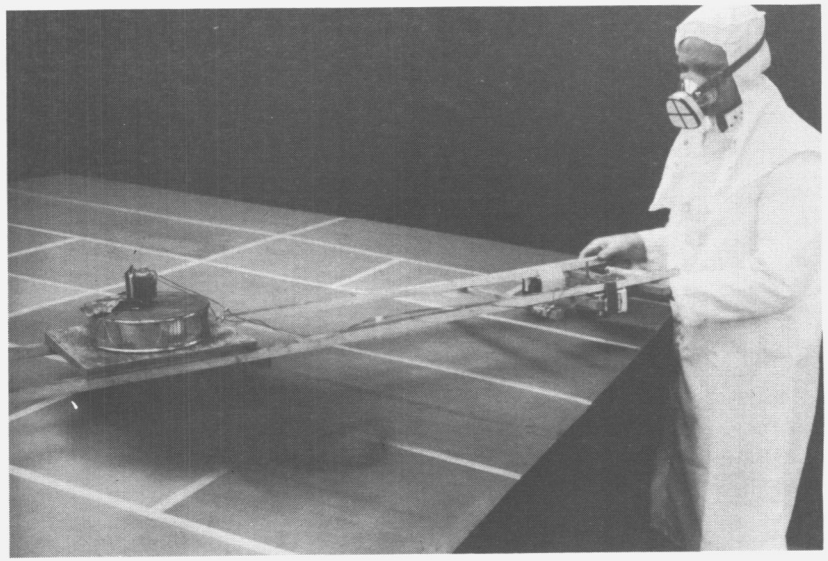

Figure 5-4. Dusting of the Model with Cupric Oxide

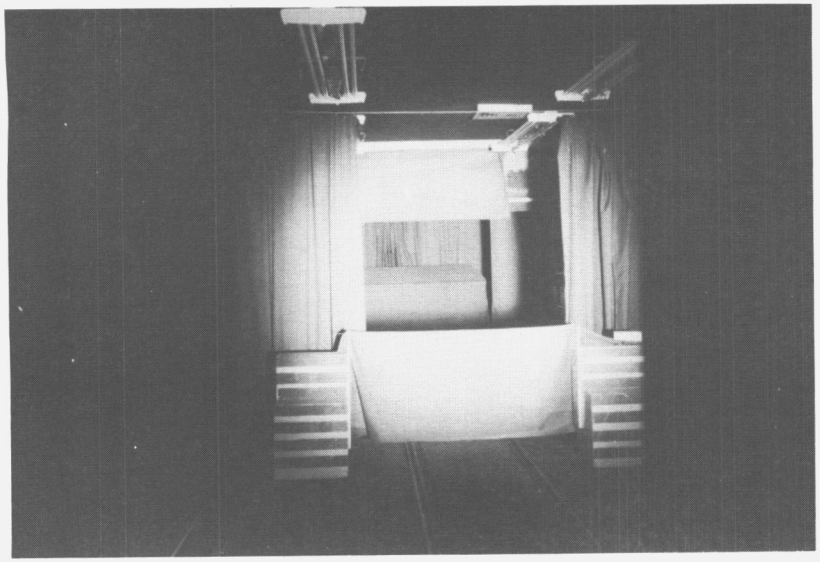

Figure 5-5. Xenon Light Beam Projected on Model Through Two Baffles

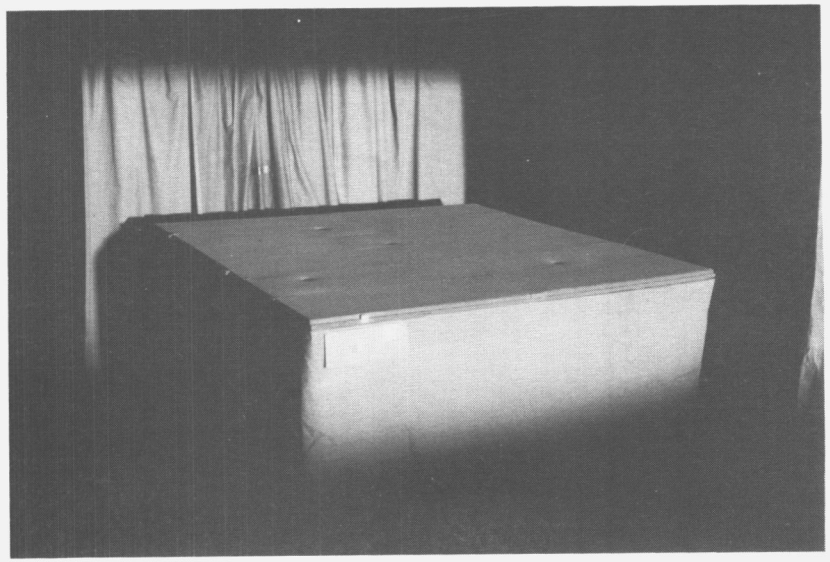

Figure 5-6. Illuminated Model with Obstacles

each of the 36 modules of the model under each of the twelve nominal sun and viewing angle combinations. These corrected azimuth, viewing angle, and range values were then employed in analyzing the data for each obstacle.

5.5 PHOTOGRAPHIC IMAGERY DEVELOPMENT

The still photograph was chosen as the means for experimental determination of the visual detectability to provide test material for the simulation study. This concept requires our taking pictures of the cupric-oxide-dusted lunar terrain model with the camera located at positions corresponding to the points on the LEM descent trajectory. The use of photographic test materials, rather than direct viewing of copper oxide dusted lunar terrain models required that care be taken to maintain within close tolerances the bright side and shadow contrast values of obstacles relative to the lunar background brightness through the numerous photographic processes to the final step in which imagery is projected on a viewing surface.

5.5.1 Technical Difficulty

The imagery of the terrain model after proper development, is expected to retain the photometric property of the photographed model when it is projected through an optical system on a screen of the simulation set-up. In order to achieve this goal, the photographic technique used to develop the imagery must possess a linear photometric relationship between the imagery projected on the simulation screen and the photographed model. This linearity must be assured for the various photographic parameters in the imagery development throughout the film processing. Significant photographic parameters in the imagery development are exposure time for both negative and positive films, light intensity, 'f' number of camera lens, developer speed, developer chemical concentration, processing, and temperature.

The first attempt at imagery development used a conventional photographic technique. This produced a developed film having very unsatisfactory photometric readings taken of the processed imagery when projected on the simulation screen. A meaningful interpretation of the film photometric property was found absolutely impossible. The processed film was considered totally unacceptable to the simulation standard established for this program which allows about 20 per cent uncertainty in the contrast between the model and imagery.

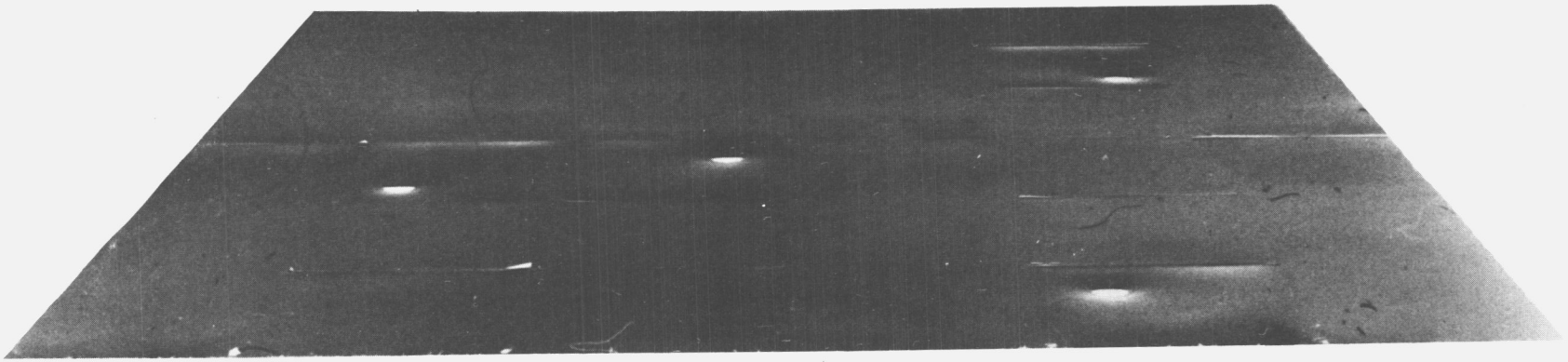

Figure 5-7. Photographic Imagery, 5 Degrees Sun Elevation, 14.4 Degrees Viewing Angle, and Zero Degrees Sun Azimuth

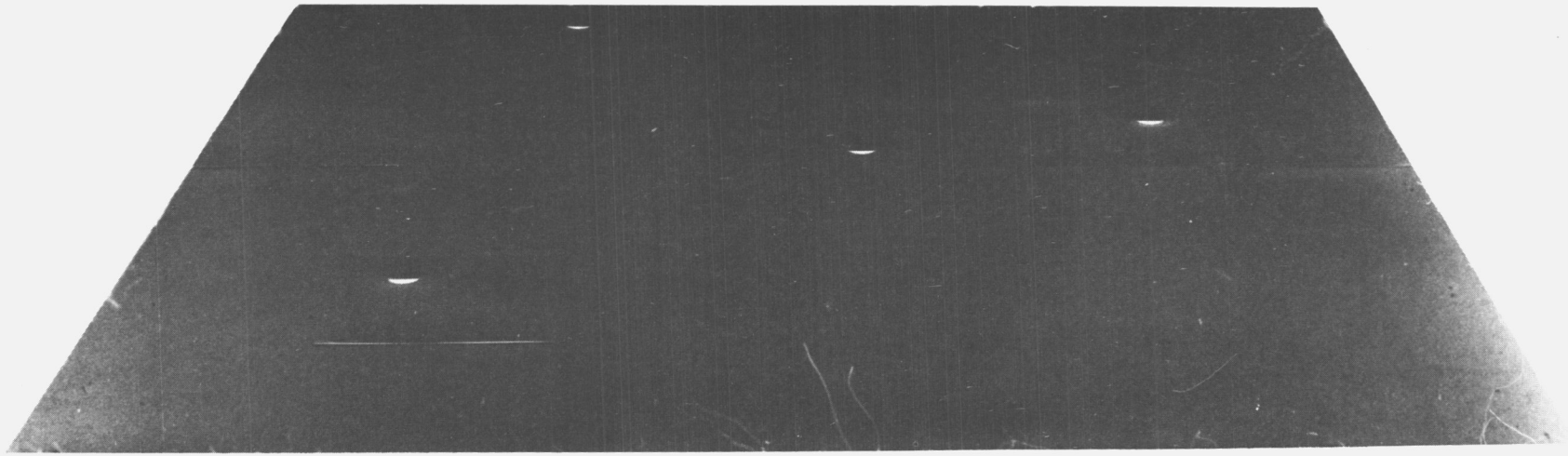

Figure 5-8. Photographic Imagery, 10 Degrees Sun Elevation, 19.8 Degrees Viewing Angle, and Zero Degrees Sun Azimuth

In short, the technical problem in imagery development was the difficulty of achieving a linear relationship between the brightness value of the cupric oxide dusted model which is photographed and that of the projected imagery of the model on a simulation screen.

5.5.2 Solution to the Imagery Development Problem

The complex imagery development was resolved by developing a new photographic technique solely for this project. This technique uses the Versamat film process machine with precision control of film (both negative and positive) development speed, chemical concentration, and processing temperature. It should be pointed out here that there is one important unique feature incorporated in this new photographic technique, i.e. correlating of the photometric relationship between CuO_2 photometric characteristics* and the J.P.L. photometric function at the sun angles and viewing geometries at which the Hughes experiments were conducted. Imagery, developed with compensation of this feature has yielded desired linear relationship between the brightness of an obstacle on the lunar surface and that on the simulation screen. Three sample pieces of the developed photographic imagery are shown in Figures 5-7, 5-8 and 5-9.

The photographic technique is explained in detail in Appendix B with steps in a sequential order.

5.6 SIMULATION TEST EQUIPMENT

A modified Carousel projector was employed to project the 35 mm. test slides onto the rear of the screen as shown in Figure 5-10. Two additional Carousel projectors were used to create the rectangular adapting field of 60 ft-L. luminance immediately surrounding the test slide. A fourth Carousel projector provided the larger surrounding field of 30 ft-L. luminance. The test image was projected within a non-illuminated band approximately 2.4 inches wide and 1.5 inches high. The arrangement of surrounding adaptation fields and dark immediate surround was a compromise solution employed to minimize contrast degradation due to stray

*data of CuO_2 photometric measurement at various sun angles and viewing geometries were furnished by NASA/MSC

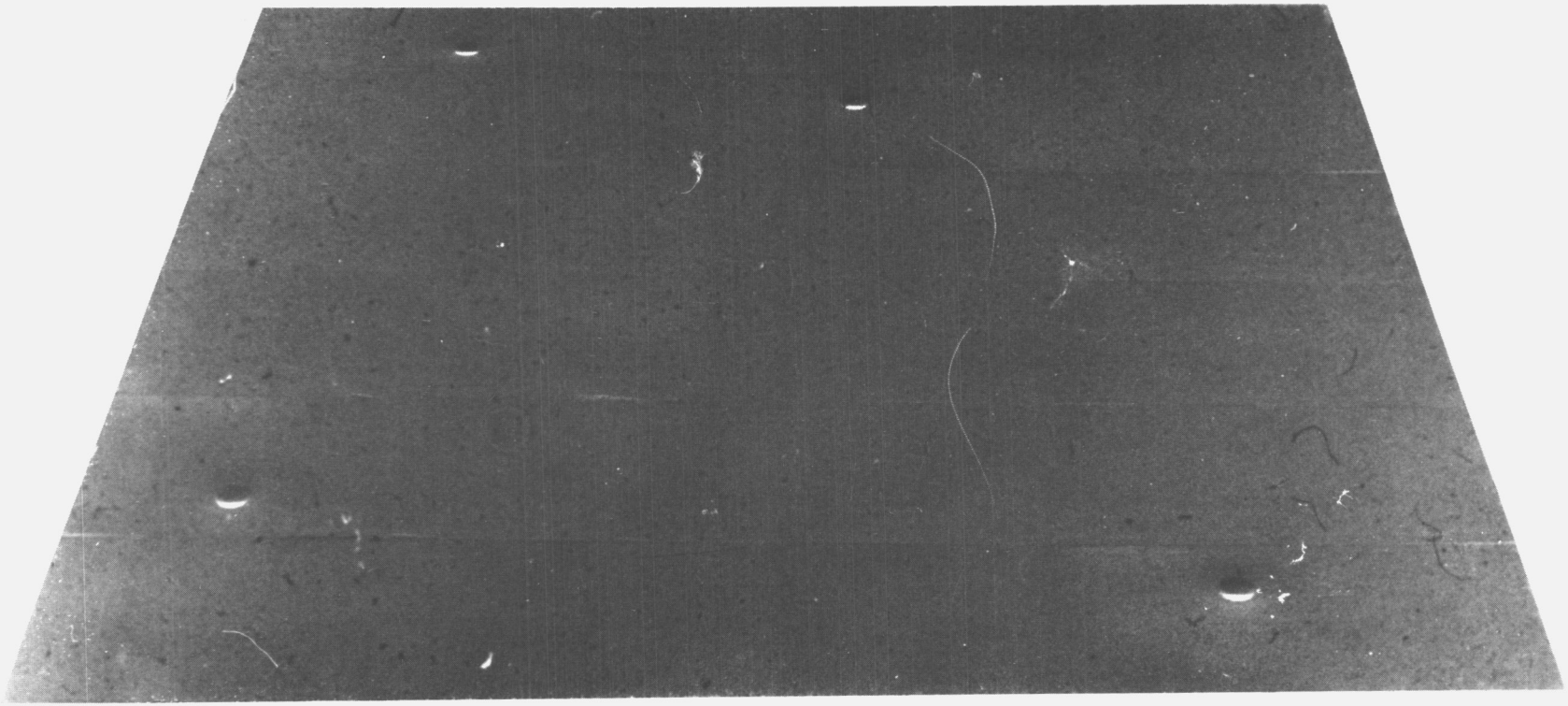

Figure 5-9. Photographic Imagery, 15 Degrees Sun Elevation, 31 Degrees Viewing Angle, and Zero Degrees Sun Azimuth

light reflections onto the viewing screen while at the same time providing enough light to maintain the adaptation of the eye to general illumination within a factor of six of terrain image background brightness.

The track and chair illustrated in Figure 5-10 were located so as to maintain the subject's head on axis to the test slide projector and thus avoid brightness changes as the chair traveled along the track.

Viewing distance to the screen was 114 inches at the far position of the chair and 18 inches at the near position, giving rise to simulated ranges of 57,700 feet to 9,100 feet. Time of travel of the motor driven chair from far to near position was 76 seconds. A constant deceleration was employed to simulate the range rate changes and search time for a representative LEM approach trajectory.

A TR-10 analog computer was employed to generate the deceleration function utilized by a motor controller to vary chair speed during travel. The analog computer also carried out the voltage integration employed to measure chair position each time the subject's toggle response switch was actuated. Voltage values were automatically read by a digital voltmeter and recorded on a digital printer.

5.7 EXPERIMENTAL PROCEDURE

The 96 test slides used in this experiment provided 4 different test slides for each of the 24 combinations of obstacle shape, spacing, sun elevation, viewing angle, and azimuth. Serial position of test conditions within the four sets was balanced.

Four subjects with normal near and far acuity, phoria, and depth perception were tested on each of the four sets of slides on different days in a balanced experimental design. A similar practice period of 24 trials preceded the experimental sessions.

On each experimental trial the test slide was revealed to the subject located at the far position on the track by opening a shutter in the optical path. One second later the chair began moving toward the screen. The chair motion continued until the subject had entered 4 obstacle detection values by actuating a spring-loaded toggle switch mounted on the chair tablet arm. At this point the chair was stopped and the subject indicated the location of each of the four obstacles, assisted by a numbered 6 x 6 matrix mounted on the tablet arm. Since the subject indicated the order in which the four obstacles had been detected, it was possible to associate each detection range voltage score with

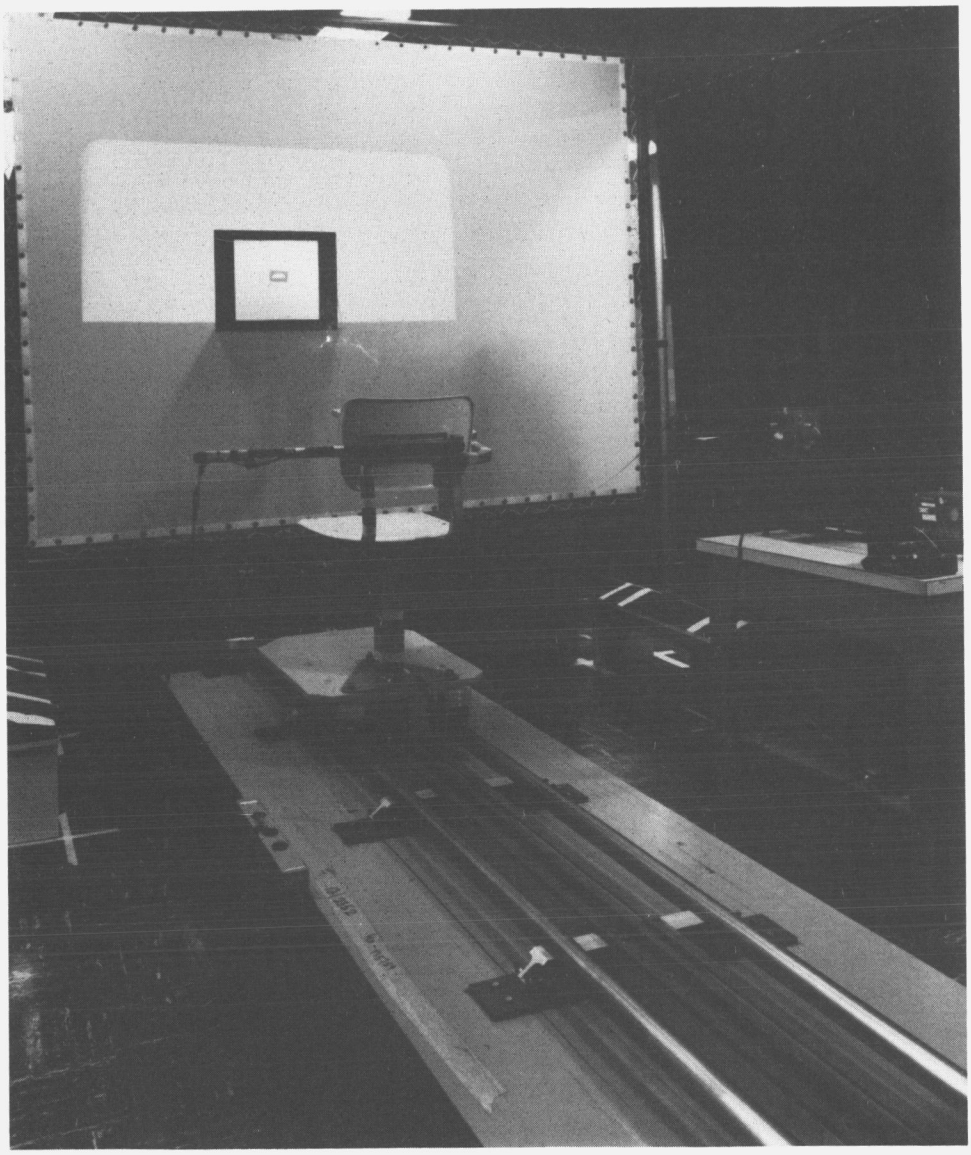

Figure 5-10. Simulation Test Track and Viewing Screen

a particular obstacle location. In 1-2% of the obstacle identifications, the subject incorrectly identified an inhomogeneity in the model, or blemish in the photographic emulsion of the slide, as an obstruction. In these cases the score was deleted, the chair was again set in motion toward the screen and the subject given additional opportunity to locate the obstacle.

6. ANALYTICAL AND EXPERIMENTAL OBSTACLE DETECTION RANGE PREDICTIONS

This section summarizes the experimentally-determined obstacle detection ranges and compares them with those derived from literature. The trends found in both results agree remarkably well, differing by a factor of approximately two, i.e. the experimental detection ranges are twice as large as the literature-based predictions. It is suggested that these results can be viewed as bounding the range of visual performance capabilities during the LEM landing approach. Conclusion derived from these findings are discussed at the end of Subsection 6.1.

As regards the LEM environmental effects which include the LEM window and astronaut face plate transmission losses, window light scatter and sun glare, the analysis has concluded that for sun elevation angles less than 30° and with the sun behind the LEM, visual performance is slightly degraded. However, all approach geometries in which the sun is in front of the LEM, provide extremely poor visual conditions for obstacle detection.

The effect of reducing contrast effectiveness due to a mottled background is discussed in Subsection 6.3. A conservative estimate of the possible degradation in lunar obstacle detection capability against a lunar terrain with significant macrostructure is given in Figure 2-8.

Additional detection range estimates for viewing angles of 9° and 55° at the sun elevations of 5, 10, 15, 30, 45, 60 and 90 degrees, and for zero and 30° azimuth angles are given in Subsection 6.4.

6.1 OBSTACLE VISIBILITY PREDICTIONS: ANALYTICAL AND EXPERIMENTAL RESULTS

In order to facilitate comparison of the results of the analytic and experimental efforts, the experimental findings are presented together with the analytical predictions for standard spherical craters and eight-sided pyramidal obstacles under similar

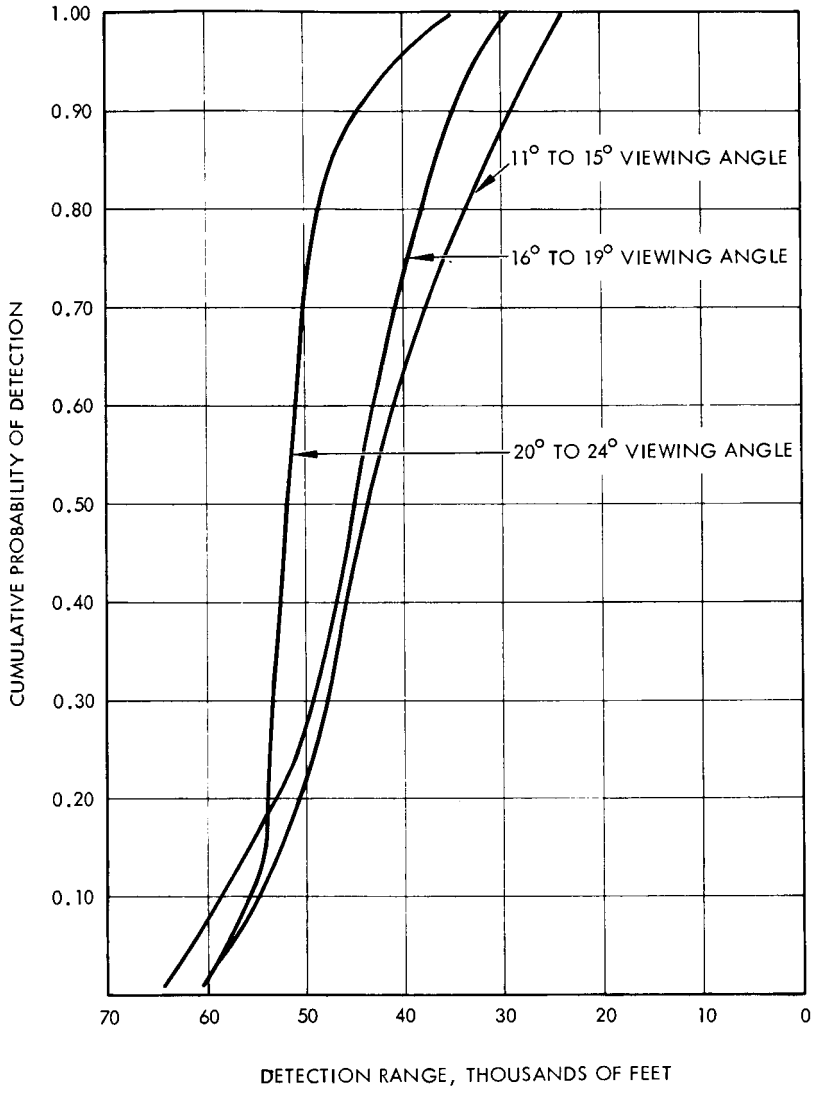

Figure 6-1. Cumulative Probability of Detection as a Function of Range

viewing conditions. These results are presented in Figures 2-1 through 2-7. Detection ranges for bright-side areas and shadows are plotted separately for the analytical predictions, while a single range value for each obstruction was derived from the experimental tests.

Two sets of predictions differ in one further respect; the analytical results are based upon the Fedoretz lunar photometric function, while the experimental imagery was developed to conform to the JPL photometric function. This is due to the fact that the analytic predictions were carried out before a shift was made to the JPL function.

The experimentally-determined detection range predictions were derived by plotting the test results as cumulative probability of detection curves, as illustrated in Figure 6-1. Range values were then read off each cumulative probability curve at the 99 percent level, the probability level employed for the analytical predictions. The complete set of data, from which the cumulative probability curves were plotted, has been submitted to NASA/MSC under separate cover.

The experimentally-determined obstacle detection ranges presented in this section have been labeled "obstacle detection ranges," consistent with the terminology employed for the analytical predictions, despite the fact that such a label is not a particularly accurate description of the experimental task or measure obtained. Detection is typically regarded as an initial or early stage in the visual process at which there is available sufficient information to signal the presence of "something" at a particular location, but not yet enough detailed information available to classify or identify the object. Detection distance or threshold is a meaningful concept in laboratory situations where a target is viewed against a uniform surrounding or in the case of night lookout tasks. Figure B-9a taken at a 5^{o} sun angle, gives an indication of the variations in background brightness, resulting from small variations in surface slope, which were visible at or before the time at which standard obstacles were discriminated. We know from our subjects' verbal reports, as well as from the small incidence of incorrect obstacle identifications, that subjects did not report "detections" but waited until they could discriminate shape and the presence of adjacent bright and dark areas characteristic of the protuberances and craters. Although the background detail was no longer visible at higher sun angles, subjects attempted to employ the same criterion for reporting an obstacle in all the experimental conditions. It is apparent, therefore, that the experimentally-determined visibility estimates reported here lie at a point well toward the "recognition" end of the detection-recognition continuum.

The most salient fact evident from a comparison of the analytical and experimental findings is that, despite the stringent criterion employed by the subjects, the experimentally-derived range estimates are generally twice as large as the literature-based predictions. It is important to establish which set of detection range estimates provide a more valid basis for LEM system decisions.

Aside from the effects of LEM environmental factors and other effects discussed in later sections of this report which can be expected to degrade visual capabilities, there are several considerations which would indicate that the experimentally-determined values are somewhat optimistic. These have to do with the size of the area to be searched for obstacles, the time available for search, and the subject's knowledge that there were four obstacles to be found in each model.

The 800-foot model subtended a small visual angle over the range of viewing distances tested, increasing from approximately 0.8 degrees at the 57,000 ft. range to 5 degrees at the nearest point. During the trial, 76 seconds were available for searching this small area. Blackwell (Reference 3) has shown that, as viewing time available for visual search for a target is increased, target detection performance is improved. The combination of small search area, extended search time, and prior knowledge of the number of targets to be located, can be expected to have yielded somewhat optimistic estimates of obstacle visibility.

There is corroborative evidence that achieving these detection ranges required extended search time. Some of the experimental data points were based on scores from two experimental conditions. In these cases an intermediate viewing angle represented the best viewing angle in a given slide and the poorest in another slide. In the first case this would often be the first obstruction which became visible and the one to which attention was first directed. Where the same viewing angle was the poorest represented in the slide, subjects would typically deal with an obstacle in that location only after identifying all others. There were very marked differences between the range scores in the two situations, indicating that with larger areas to search and less time to spend searching a given area, detection ranges will be smaller than those found under these experimental conditions.

For these reasons, the experimental and analytical results can be viewed as bounding the range of visual performance capabilities during the LEM approach, neglecting environmental effects and other adverse factors. The experimentally-determined values apply to visual search of a small, well-defined area such as the immediate vicinity of programmed touchdown point, to which considerable time (on the order of 30 seconds), is devoted for visual search.

The more conservative analytical estimates apply to more hurried search of larger areas, where the astronaut is rapidly scanning for an alternate or more favorable landing area.

Aside from these differences in the absolute level of obstacle detection ranges, the general agreement between the two sets of data is good. Comparison of the shapes of the curves for the two sets of data indicates that the experimentally-derived detection ranges fall off with increasing sun angle in very much the same fashion as the literature-based shadow estimates. The two sets of curves are thus in good agreement in demonstrating the superiority of low sun angles over the full range of viewing angles investigated.

It was stated earlier that the experimentally-derived obstacle visibility estimates are approximately twice as large as the literature-based predictions. It is of interest to examine quantitatively this relationship for cases allowing comparison between the two sets of predictions in order to judge the regularity of the differences. A rough comparison is the best that can be managed because of the different lunar reflectivity models employed and the grouping of experimental data within 3 and 4 degree intervals of viewing angle. In Table 6-1 analytically-derived estimates for spherical craters at viewing angles of 14.4 and 18.4 degrees and azimuth angles of 0 and 30 degrees are presented. These values are compared with experimentally-derived scores for the 11-15 and 16-19 viewing-angle intervals, choosing in each case from the bright side and shadow ranges that score giving the larger detection range estimate. The experimental scores for the 30 degree azimuth comparisons are mean values averaged over the 16-30 and 31-45 degree azimuth intervals, while experimental scores for the 0-15 degree azimuth intervals are compared with analytical zero azimuth values. Comparison on this basis can be justified on the following grounds:

1) Differences between the Fedoritz and JPL lunar reflectivity models are not appreciable in estimating visibility under the lighting and viewing conditions examined.

2) Grouping of experimental scores into the viewing and azimuth angle intervals employed gives rise to range estimates based on a reasonably large number of data points.

It can be seen in Table 6-1 that, for these comparisons between experimental scores and the larger of the analytical bright side and shadow range estimates, the ratios for the individual comparisons do not deviate markedly from the mean ratio of 2.12. It should be noted that the greatest departures are found with a sun angle of 15 degrees.

TABLE 6-1

Comparison of Experimental and Analytical Detection Ranges for Spherical Craters Employing Higher Value of Bright Side or Shadow Analytical Predictions

Sun Angle (Degree)	Azimuth (Degree)	R_A Analytical Detection Range Thousands of Feet	R_E Experimental Detection Range Thousands of Feet	$\frac{R_E}{R_A}$
		18.4° View Angle	16-19° View Angle	
5	0	14.9	30.7	2.06
	30	15.1	29.0	1.92
10	0	12.2	19.9	1.64
	30	10.3	27.4	2.62
15	30	5.4	16.8	3.11
		14.4° View Angle	11-15° View Angle	
5	0	15.3	26.6	1.74
	30	13.4	27.0	2.01
10	0	9.2	11.4	1.24
	30	8.7	10.4	1.20
15	30	3.6	13.9	3.86
			Mean Ratio of $\frac{R_E}{R_A}$	2.12

Further insight into the relationship between these analytical and experimental estimates of obstacle visibility is possible if account is taken of differences at the three sun angles in both the obstacle detection task and the information required to discriminate obstacles. Inspection of Fig. 5-7 thru. 5-9 reveals the amount of detail due to minor irregularities in the surface of the terrain models which was visible at a sun angle of 5 degrees and, to a lesser extent, at 10 degrees. At a sun angle of 15 degrees these minor imperfections in the surface of the models were no longer visible either in direct vision or in the photographic imagery. The spontaneous comments of the experimental subjects indicate that at the lower sun angles it was necessary to distinguish the presence of both shadow and bright side in order to discriminate obstacles from other surface inhomogeneities. Under these conditions, obstacle identification at a 5 or 10 degree sun angle would be delayed until both shadow and bright side of the crater were discriminated. At the highest sun angle, however, identification of either detail would provide an adequate basis for obstacle identification, since any inhomogeneity visible on the surface would be a sufficient cue.

In view of the above, it is of interest to compare the experimental results with the less visible obstacle detail, i.e. the lesser of the analytical bright side or shadow range estimates for each of the conditions listed in Table 6-1. The results of this comparison are presented in Table 6-2. It can be seen that at 5 and 10 degree sun angles, the experimental-to-analytical ratios show somewhat closer agreement than was evident in Table 6-1. The mean ratio for these two sun angles is 2.18. In contrast, the ratios for the 15 degree sun conditions are appreciably higher.

In order to adequately evaluate these findings, it is necessary to distinguish between aspects of the simulation test situation peculiar to the test conditions employed and those which have greater relevance toward prediction of lunar obstacle visibility. The greater discrepancy between experimental and analytical estimates at a 15 degree sun angle is attributable to the subjects' a priori knowledge that there were four obstacles present in each test slide. In contrast, the surface inhomogeneities visible at lower sun angles in the test imagery more closely approximate known characteristics of the lunar terrain than would a completely smooth, homogeneous surface. The experimental data for 5 and 10 degree sun angles, as well as the relationship between analytical predictions and the test results for these lower sun angles, thus provide the most relevant basis for lunar visibility predictions.

Another comparison of interest is that between visibility estimates for single obstacles and closely spaced groups of four craters or protuberances. Since a single obstacle in an otherwise level area can be easily avoided by a small maneuver shortly before

TABLE 6-2

Comparison of Experimental and Analytical Detection Ranges for Spherical Craters Employing Lower Value of Bright Side or Shadow Analytical Predictions

Sun Angle (Degree)	Azimuth (Degree)	R_A Analytical Detection Range Thousands of Feet	R_E Experimental Detection Range Thousands of Feet	$\frac{R_E}{R_A}$
		18.4^o View Angle	$16\text{-}19^o$ View Angle	
5	0	12.4	30.7	2.50
	30	13.9	29.0	2.09
10	0	9.5	19.9	2.10
	30	9.0	27.4	3.03
15	30	3.8	16.8	4.42
		14.4^o View Angle	$11\text{-}15^o$ View Angle	
5	0	12.9	26.6	2.06
	30	12.5	27.0	2.16
10	0	7.7	11.4	1.50
	30	5.2	10.4	2.00
15	30	1.7	13.9	8.18

landing, it should not pose a serious threat to mission safety. Test slides containing groups of obstacles were therefore included in the simulation test as a more realistic obstacle avoidance condition to ascertain whether significant differences in detection range would be found between individual widely-spaced obstacles and clustered groups. The two conditions were compared by averaging range scores over all common lighting and viewing geometries. It was found that detection ranges for groups of 4 craters were approximately 10 per cent greater than those for individual craters, while the equivalent value for protuberances was 20 per cent. However, the terrain model sections containing four obstacles showed some deformation of the area surrounding obstacles resulting from the thermoplastic forming technique employed. Although these modest differences between the scores for single obstacles and groups cannot be accepted at face value because of the possibility that they are due to an experimental artifact, it appears that there are no important differences in obstacle visibility between the two conditions.

Further sections of this report consider the effects of other factors which can be expected to alter somewhat the relationships among sun and viewing angles in determining obstacle visibility which have been presented in this section. Before summarizing the results of these analytical and experimental efforts and proceeding to consideration of some LEM environmental effects and lunar terrain characteristics important to visibility, it is of value to examine further the consistencies and discrepancies between the experimental and analytical findings. The purpose of such an examination is that of assessing what these results contribute toward evaluating the usefulness of analytical procedures based on laboratory psychophysical studies in predicting visibility in complex visual identification tasks.

It can be stated unequivocally that the basic psychophysical data and field factor corrections derived from the work of Blackwell, together with the techniques employed to estimate contrast and area values, were of major value in initially identifying the range of more favorable illumination and viewing conditions. It was possible on this basis to focus the simulation test effort on low sun angles, rather than attempt to gather experimental data for a wide range of viewing conditions.

The evidence reviewed here indicates good agreement between the experimental and analytical results in defining the shape of the function relating area and contrast values to obstacle discrimination. Although it is difficult to partial out the relative contribution of individual variables in complex interaction, the lack of gross differences in the pattern of results between the two sets of data indicates that the basis for estimating effective size and contrast of bright side areas was reasonably well chosen.

The analytical prediction of greater visibility of shadow areas relative to bright side for most conditions was in agreement with subjective impressions in viewing the imagery.

If it is granted that the general pattern of results, i.e. the shapes of the curves, show reasonably good agreement, then the difference in absolute values is attributable either to the field factors of 15.0 and 18.6 applied in the Tiffany Foundation data for this application, or to summation between adjacent areas of negative and positive contrast (shadow and bright side) resulting in increases in effective contrast over those predicted. The information available is not sufficient to permit a choice between these alternatives.

A word of caution is required concerning the extent to which the absolute values of obstacle detection ranges derived from the simulation tests can be employed to predict astronaut performance capabilities in obstacle identification during terminal states of the LEM landing approach. It must be emphasized that the limited scope of this study made it necessary to deal with a bounded problem in which it was necessary to ignore many aspects of the full task of landing site selection. The simulation tests employed a limited range of obstacle sizes and shapes, employing idealized obstacles for which no attempt was made to represent the range of obstacle shape inhomogeneities and variations anticipated on the lunar surface. Similarly, it was not possible to require judgments of obstacle size or depth, such as will be required in landing site selection. These additional complexities of the site selection task attributable to the perceptual tasks not included in this study can be expected to increase the time required for visual search of the landing area, with some concomitant reduction in obstacle detection ranges. Although the results of this study have established an optimum range of illumination and viewing conditions, additional study is required in order to take into account the effect of those additional factors on obstacle identification capabilities as they affect detailed planning of the LEM mission. Some important areas in which such additional analysis and study are indicated to supplement the results obtained in this program are presented in Section 8.6.

Several significant conclusions may be derived from these data:

(1) Longer detection ranges are found at low sun angles.

(2) Detection ranges increase with higher (steeper) viewing angles for all sun angles studied.

(3) Viewing angles greater than 25 degrees are necessary to insure moderate obstacle visibility at 0-15 azimuth for sun elevation angles in the vicinity of 15 degrees.

(4) The contribution of azimuth differences between sun and viewing position to the effective phase angle permits a somewhat lower viewing angle of about 20 degrees to be employed with a 15-degree sun while still retaining moderate obstacle visibility.

(5) Detection range differences between protuberance and crater, as well as those between single obstructions and clustered groups of four, are relatively small as compared to the effects of sun and viewing angle variations.

6.2 LEM ENVIRONMENTAL EFFECTS ON OBSTACLE VISIBILITY

A set of detection range predictions were prepared spanning the full range of sun angles from behind the LEM to directly ahead. In addition to range predictions in the form previously presented, the effects on crater visibility were predicted for the optical scatter and transmission characteristics of the LEM window, pressure suit face plate transmission losses, and sun glare for geometries in which the landing approach is made into the sun. These analyses utilize a window scatter value of 10 percent, a somewhat pessimistic, although realistic estimate of the probable degradation of visibility from reaction control system thrusters, provided us by cognizant MSC personnel. The light transmission loss values employed are 20 percent for the LEM window, and 10 percent for the face plate. The effects of solar glare on detection were estimated by employing the data of Holladay (Reference 7) in which a peripheral glare source is equated to a veiling luminance interfering with visibility to the same degree. Holladay found the following equation to hold:

$$B_V = \frac{9.2\ E_o}{\theta^2}$$

where B_V = veiling luminance in candles per square meter

θ = angular separation in degrees between glare source and fixation point

E_o = illuminance in lumens per square meter in the plane of the eye

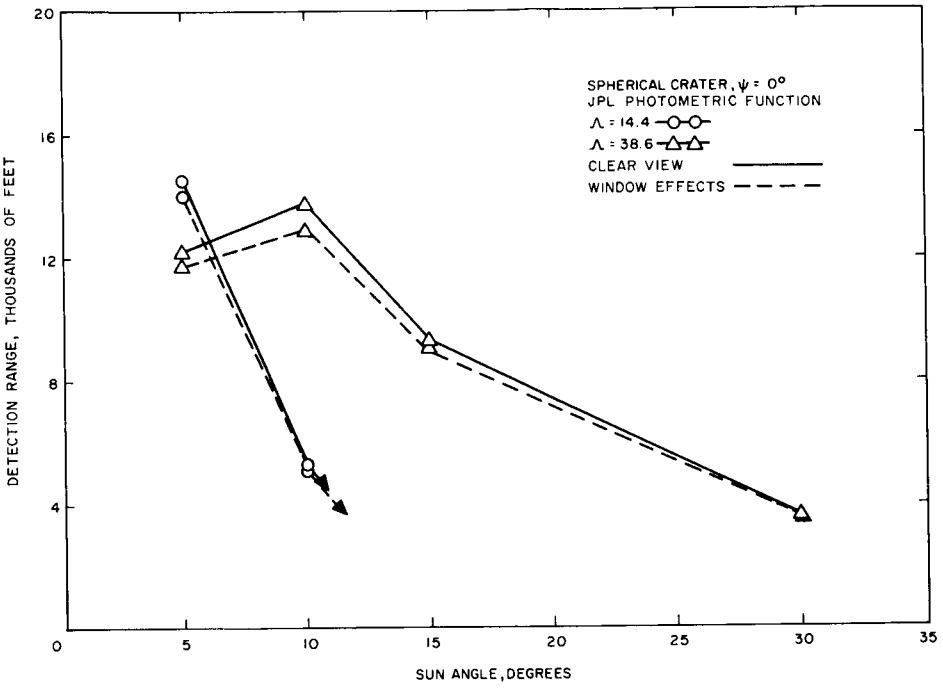

Figure 6-2. Bright Side Detection Range of Lunar Obstacle versus Sun Elevation Angle with Veiling Luminance Effects - Spherical Crater, Zero Azimuth

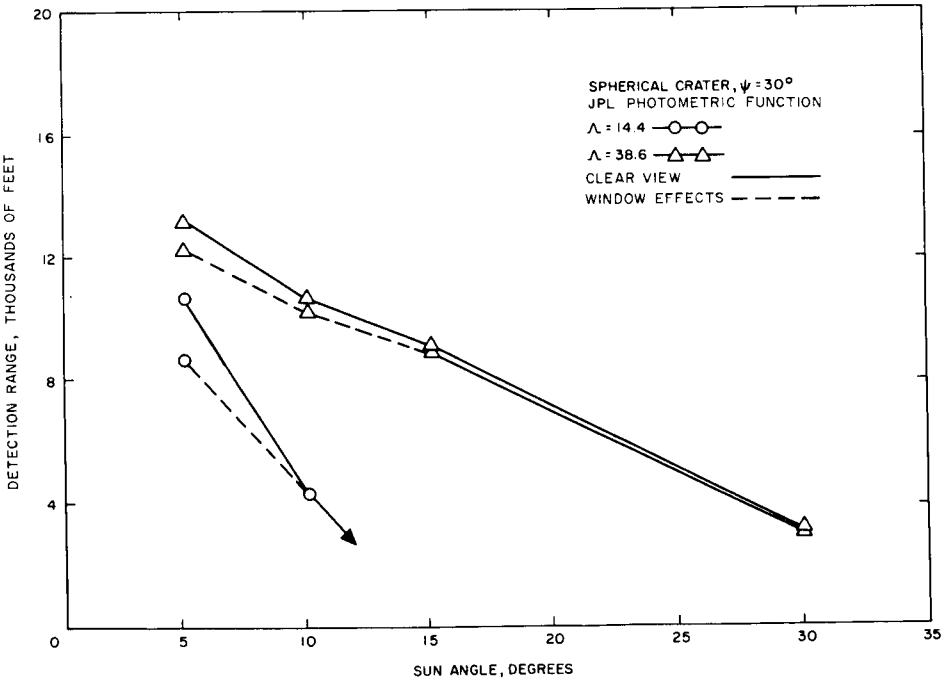

Figure 6-3. Bright Side Detection Range of Lunar Obstacle versus Sun Elevation Angle with Veiling Luminance Effects - Spherical Crater, 30 Degrees Azimuth

The results presented in Figures 6-2 through 6-5 were computed for a pitch orientation of 43 degrees, representative of vehicle orientation at high gate. Two viewing angles, 14.4 and 38.6 degrees were considered. The curves show that window scatter and transmission losses have relatively little effect on detection range estimates over the 5-30 degree range of sun angles for which data are plotted. At sun angles between 30 and 180 degrees, contrast values are not sufficient to permit obstacle detection. Between 90 and 180 degrees, solar illumination falling on the window, or the visibility of the sun in the window, creates contrast degradation and veiling glare effects sufficiently intense to preclude obstacle detection at most sun angles. The only exceptions are at a sun elevation of 150 degrees, where horizontal detection range for crater bright side is estimated at 2170 feet, and at 165 degrees, where crater shadows provide an estimated range of 1920 feet. These results indicate that all approach geometries in which the sun is in front of the vehicle provide extremely poor visual conditions for obstacle detection.

6.3 LUNAR SURFACE MICROSTRUCTURE VERSUS MACROSTRUCTURE

The Lunik IX and Surveyor photographs revealed lunar terrains in which surface irregularities and boulders give rise to highlights and shadows visible at appreciable distances. There is evidence that complex background of this type interferes with the detectability of large objects and areas of contrast. The degree to which obstacle identification will be degraded due to lunar terrain macrostructure, where surface irregularities adjacent to craters and cones range in size between 1 and 2 feet, is difficult to estimate without experimental tests. A lower boundary to the decrement which may be expected can be derived from a study by Blackwell and Bixel (Reference 8), in which a conversion factor was sought to relate effective contrast for non-uniform backgrounds to threshold contrast values for uniform backgrounds. It was found that the average contrast between mottled backgrounds and uniform targets was less effective for target discrimination than equivalent contrast of uniform luminance. For those experimental conditions in which size relations between background detail and target dimensions approximated lunar conditions, conversion factor values were obtained using two different psychophysical test procedures. The contrast effectiveness of a mottled background was found to be 0.70 and 0.51 of equivalent uniform luminance when the two test procedures were applied.

The effect of reducing contrast effectiveness by these values on predicted obstacle detection range is shown in Figure 2-8, in which detection range at 7 degrees sun elevation for a 11.36 to 1 cone of 2 foot height is plotted as a function of observer viewing angle.

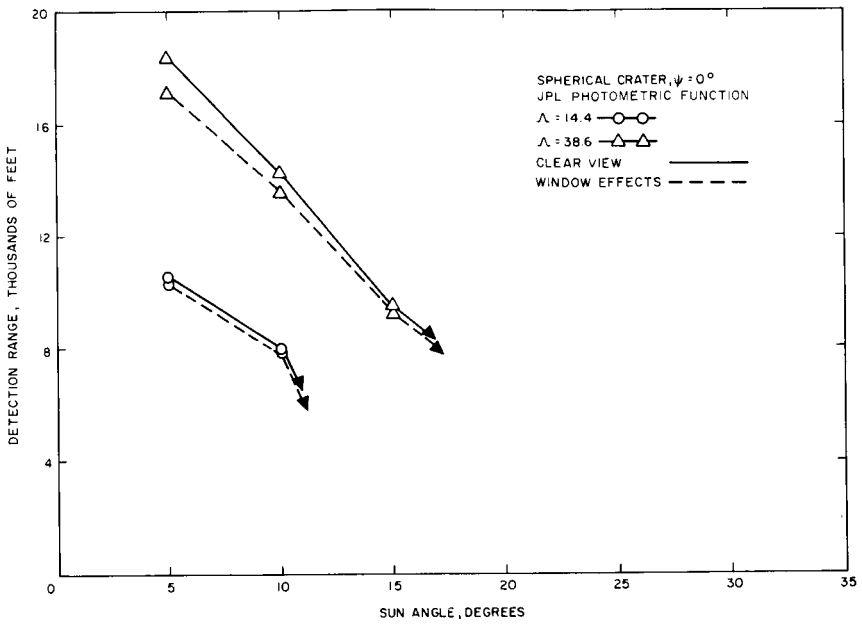

Figure 6-4. Shadow Detection Range of Lunar Obstacle versus Sun Elevation Angle with Veiling Luminance Effects - Spherical Crater, Zero Azimuth

CRATER SHADOW DETECTION RANGES VS. SUN ELEVATION ANGLE
WITH AND WITHOUT OPTICAL TRANSMISSION AND SCATTER EFFECTS

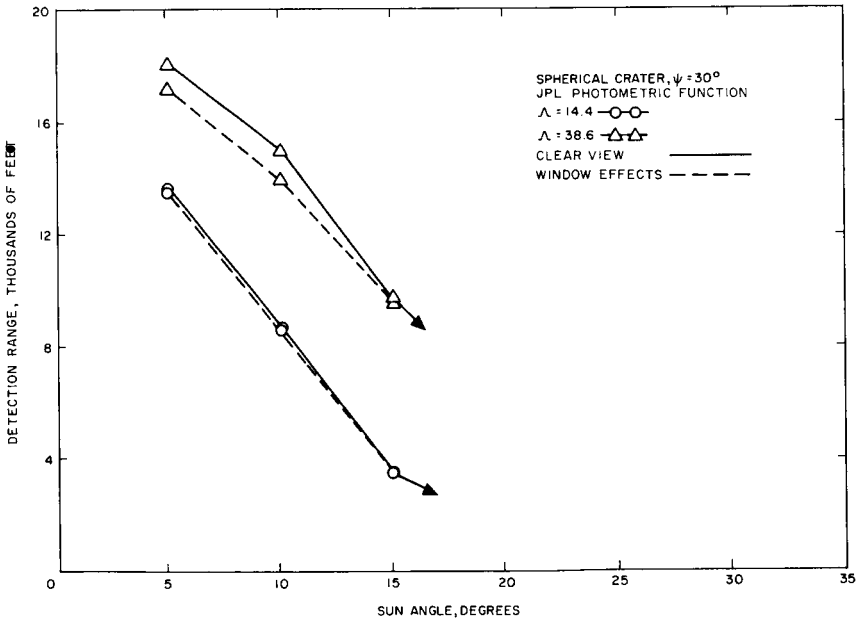

Figure 6-5. Shadow Detection Range of Lunar Obstacle versus Sun Elevation Angle with Veiling Luminance Effects - Spherical Crater, 30 Degrees Azimuth

The significant reduction in detection range shown in Figure 2-8 is a conservative estimate of the possible decrement in obstacle detection capability against a lunar terrain with significant macrostructure, since similar roughness of the surface of terrain features large enough to constitute landing hazards would further reduce effective contrast values and detection range predictions.

6.4 DETECTION RANGE ESTIMATES FOR 9^{o} and 55^{o} VIEWING ANGLES

Obstacle detection range estimates for the viewing angles of 9 degrees and 55 degrees, at sun elevation angles of 5, 10, 15, 30, 45, 60 and 90 degrees and for sun azimuth angles of zero and 30 degrees are shown in Figure 6-6 for the bright-side detection. The obstacle, used for the estimate, is a 10-degree slope, 8-sided cone which is concave-shaped for crater and convex-shaped for protuberance. The J.P.L. photometric function is employed for the computer run to generate the contrast values.

The shadow detection ranges can be estimated only for low sun elevation angles of 5^{o} and 10^{o} because the shadow exists only at sun elevation angles less than 10^{o} due to the factor that the side slope of the 8-sided pyramid obstacle is 10^{o}. Since the estimated shadow detection range data available are insufficient to plot the curves for establishing its trend, it is decided to give these data in Table 6-3.

The bright-side detection for 9^{o} viewing angles has indicated insufficient contrast for practically all sun angles except about the 5^{o} sun elevation angle. This clearly points out that the sun angle greater than viewing angle yields unfavorable lighting condition. The curves in Figure 6-6 show a favorable situation for the higher viewing angles. They also indicated that with the sun elevation angles larger than 15^{o}, the bright side contrast of the obstacle is about the same for both the craters and protuberances. Therefore, detection ranges for both obstacle shapes are identical.

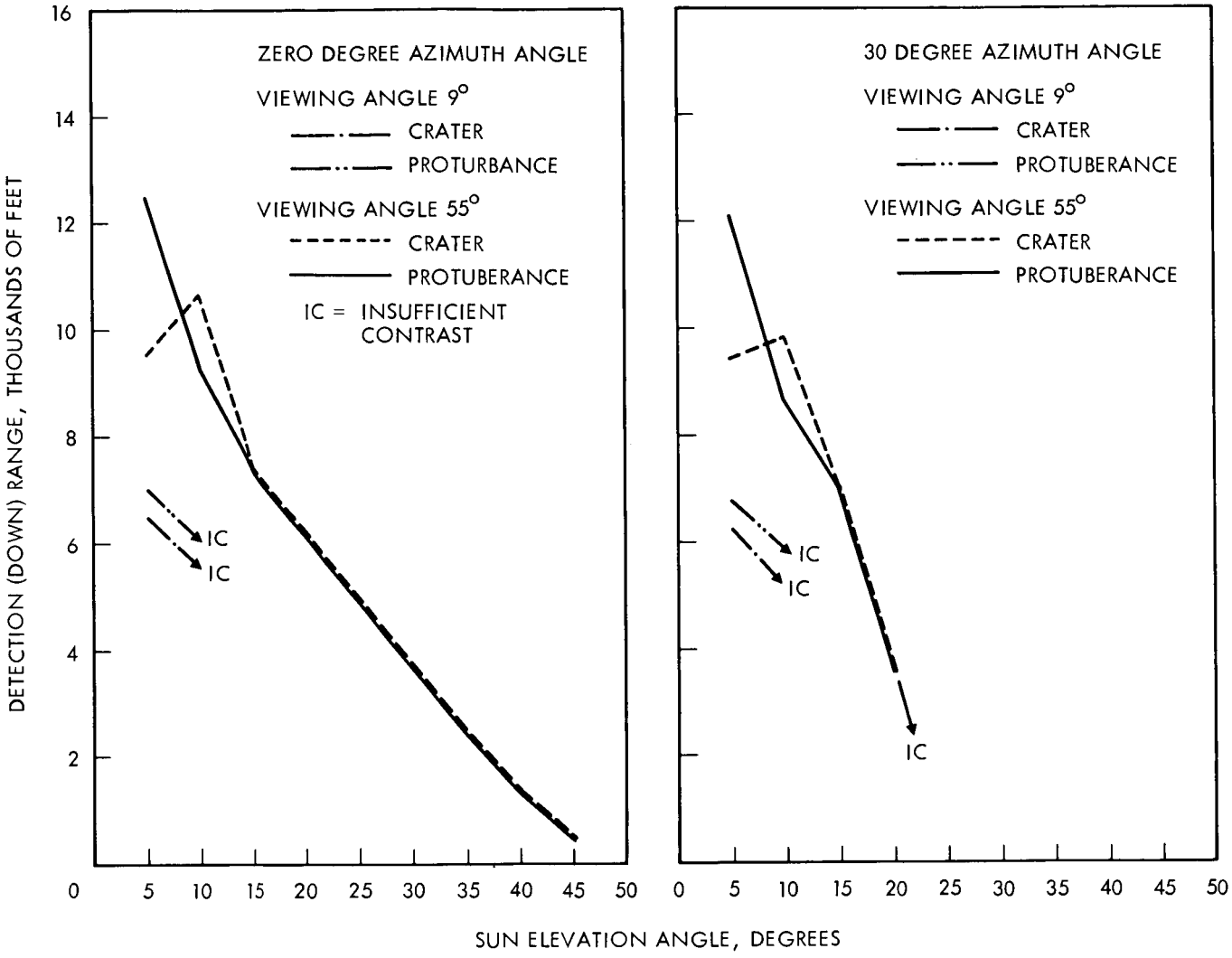

Figure 6-6. Bright Side Detection Range for Eight Side Cone-Shaped Obstacle Based on JPL Photometric Function

TABLE 6-3

Shadow Detection Ranges for Eight-Sided Cone-Shaped Obstacle Based on J.P.L. Photometric Function

Sun Elevation Angle Degrees	Viewing Angle Degrees	Sun Azimuth Angle Degrees	Detection Range Feet
		Protuberance 	
5	9	0	15,376
5	9	30	16,949
5	55	0	21,959
5	55	30	22,223
10	9	0	no shadow
10	9	30	5,820.8
10	55	0	14,030
10	55	30	13,683
		Crater 	
5	9	0	8,231.8
5	9	30	8,932.8
5	55	0	14,491
5	55	30	13,944
10	9	0	no shadow
10	9	30	4,115.9
10	55	0	11,799
10	55	30	11,799

7. OPTICAL AIDS ANALYSIS

On cursory inspection, it would appear that the use of binoculars or other optical aids might be expected to markedly improve obstacle visibility during the LEM terminal approach. The visibility nomograph presented in Figure 4-1 shows that except for marginal contrast values, visual size is a more potent factor than contrast in determining detection capabilities. The theoretical improvement in detection range, neglecting other factors, to be expected from optical magnification aids is in general equal to the 2/3 power of the magnification employed.

There are several factors, however, which can be expected to minimize the value of optical magnification. These include: (1) the increase in search time required to scan a given terrain area resulting from the smaller area which can be scanned in a single visual fixation, (2) the difficulty of carrying out an orderly search of the terrain with a limited field of view, particularly if the astronaut must interrupt visual search for other time-shared activities such as instrument monitoring, (3) orientation problems in relating what is seen by means of the optical aid to the visual scene apparent in unaided vision if distinctive landmarks are not present in the magnified image, and, (4) the increased vulnerability to degradation of visual acuity due to vehicle vibration and hand tremor, compounded by the difficulty of locating the exit pupil of the optical aid close to the eye if the pressure suit visor is worn.

In view of these difficulties, it is well first to consider the lighting and viewing geometries for which magnification could prove of value. The results of this study indicate that it is only at low sun angles up to a maximum of approximately 15 degrees that contrast values are adequate for obstacle visibility at feasible viewing and trajectory angles; image magnification can be of no assistance in the absence of obstacle-background brightness differences or in the presence of veiling glare. The question then boils down to whether, at or close to 15 degrees, an optical aid will allow for higher sun angles or a shallower approach trajectory than would otherwise be possible.

The optical aid could be of some slight assistance for early inspection of the programmed landing site, permitting earlier identification of obstacles, if means are available for locating the landing site accurately. Although it might thus be feasible to employ an optical aid for initial inspection of a small portion of the landing area, it would be of little or no value beyond this point in the landing approach. If the designated touchdown point is unsuitable, it will be necessary to select a more favorable area in time to institute the maneuvers required for alteration of the trajectory. The additional time required for search with magnification, the greater potential for inefficient search procedures with the optical aid, and the possibility of "losing" a promising area when switching to unaided vision, all argue against the suitability of optical aids where visual search must be carried out under stringent time pressures with little leeway for confusion or error. Selection of suitable sun and approach trajectory angles, and utilization of an optimum strategy for the order in which various locations in the landing footprint are searched, as described in Section 8, appear to be more promising means of insuring that decisions concerning landing area suitability are precise and timely.

8. CONCLUSIONS AND RECOMMENDATIONS

Interpretation and application of the findings of this study toward selection of optimum and acceptable ranges of lighting conditions and viewing geometries are presented in this section. Implications for alteration of the LEM approach trajectory are discussed, as well as those leading toward development of optimal visual search strategies for landing point selection. Some areas are listed in which analysis and study would do much to supplement and extend the results of this program in predicting obstacle visibility and in selecting optimum viewing conditions and search techniques for landing area selection.

8.1 OPTIMUM SUN ANGLES

Both the experimental and analytical findings indicate that optimum sun elevation angles for obstacle detection are found between 5 and approximately 8 degrees. Large obstacle shadows combine with excellent bright side contrast to provide very large detection ranges over all viewing and azimuth angles studies. Of equal importance is the fact that in our test imagery these low sun angles appear to provide distinctive indications of terrain slope and macrostructure not visible at higher sun angles. The only constraint upon unequivocal recommendation of these low sun angles from the standpoint of visual capabilities is concerned with the flatness of the lunar topography in the immediate vicinity of the landing area, since adjacent hills and ridges will cast elongated shadows within which all detail is invisible.

8.2 OPTIMUM VIEWING ANGLES

The longest detection ranges are obtained with viewing angles higher than sun elevation. Results of this study indicate that the benefit of higher viewing angles extends at least to 30 degrees above the sun elevation, indicating that LEM approach trajectory values of 10 - 20 degrees are not optimum for landing point selection, particularly for sun angles above 5 degrees.

8.3 ACCEPTABLE COMBINATIONS OF SUN AND VIEWING ANGLES

Although the results of this study indicate how visibility for a given sun or viewing angle can be improved by proper selection of the overall lighting-viewing geometry, we do not have all of the information required to specify the limit values of the range of acceptable sun and viewing angles. This is the case because detailed specification of acceptable values depends upon astronaut work load and time sharing requirements during the terminal approach, as well as on time requirements for implementing a decision to designate a new touchdown point. In the absence of such information, it is possible only to summarize the relationships found within the results of the study, without a sharp and clear delineation of the limits for the acceptable range of values.

The curves presented in Section 6.2 indicate that above a sun angle of 15 degrees all shadow information is lost for standard obstacles with gently-sloping sides. For sun angles between 15 and 30 degrees, bright side contrast permits some residual obstacle detection capability, but only at viewing angles considerably above the current maximum LEM trajectory angle of 20 degrees. A sun angle of 15 degrees or slightly less thus appears to represent the highest sun angle value which should be considered. If a sun angle at or near 15 degrees must be employed, higher viewing angles are mandatory, and consideration should be given to the use of a dog-leg maneuver to take advantage of the lower viewing angles permissible with a 30-45 degree azimuth angle.

8.4 RECOMMENDED TRAJECTORY CHANGES

The preceding paragraphs have pointed out the desirability of increasing viewing angles, and thus the LEM trajectory, above the current maximum value of 20 degrees.

8.5 VISUAL SEARCH STRATEGY

Devising a visual search strategy specifying the order in which various locations in the landing footprint are to be searched as well as the amount of time devoted to search of each area, would require taking into account astronaut work load, expected terrain characteristics, and the amount of pre-flight information concerning the landing area. The results of this study nevertheless provide some important contributions toward an optimum search strategy. The curves presented here demonstrate that there is little or no point in searching beyond the expected touchdown point since longer viewing distances and shallower viewing angles will delay obstacle detection in this region of the footprint.

For many sun and viewing angle combinations, it will be possible to search for and select an alternate landing site before it is possible to determine the suitability of the area directly ahead toward which the trajectory is directed. Similarly, it is possible to use the present results to construct a priority list of locations in which a suitable alternate landing area should first be sought in the event that the intended landing point is found to contain landing hazards.

8.6 IMPORTANT SIMULATION WORK SUPPLEMENTAL TO THIS PROGRAM IN VISUAL SELECTION OF LEM LANDING SITE

The following are judged to be important areas to which analysis and study should be devoted to extend and supplement the results obtained in this program:

8.6.1 Terrain Slope Estimation, Obstacle Size Estimation, and Search Time

The Lunik IX and Surveyor photographs reveal a terrain in which surface irregularities and boulders give rise to highlights and shadows visible at appreciable distances. There is evidence that complex backgrounds of this type interfere with the detectability of larger objects and areas of contrast. Simulation tests should be carried out with terrain models including such surface macrostructure in order to assess the influence of complex surfaces on obstacle detection, obstacle size estimation, slope estimation, and search time.

8.6.2 LEM Environmental Effects on Visual Capabilities

Additional study should be devoted to environmental effects, including window transmission and scatter characteristics with thruster deposits, and the effects of the LEM vibration spectrum evaluated in shake-table tests.

8.6.3 Search Strategy and Decision Making

Search, detection, and decision time should be studied as a function of available viewing time, time sharing requirements and other workload and time requirements for implementing decisions. These studies are required to devise efficient search strategies and to estimate the ranges at which it will be possible to arrive at final decisions concerning landing area suitability.

9. REFERENCES

1. Hughes Aircraft Company, "Midterm Report, A Study to Determine Optimum Lunar Lighting Conditions for Visual Selection of LEM Touchdown Point." For NASA/MSC Houston, Texas under Contract NAS 9-5321. February, 1966. Hughes SSD 60059R.

2. H. R. Blackwell, "Contrast Thresholds of the Human Eye." J. Opt. Soc. Amer., 36, 624-643 (1946).

3. H. R. Blackwell, "Development and Use of a Quantitative Method for Specification of Interior Illumination Levels," Illum. Eng., June, 1959.

4. W. R. Fox, "Visual Discrimination as a Function of Stimulus Size, Shape, and Edge Gradient," Boston Univ. Physical Res. Lab., Technical Note No. 132, August 1957.

5. A. B. Kristofferson and R. H. O'Connell, "Detectability of Targets Containing Internal Luminance Gradients," University of Michigan Research Institute, Project MICHIGAN, Report No. 2144-297-T, 1958.

6. "Natural Environment and Physical Standards for the Apollo Program," NASA Washington D.C. 20546 M-D E8020.008B SE 015-001-1.

7. L. L. Holladay, "The Fundamentals of Glare and Visibility," J. Opt. Soc. Am. 12, 271-319, (1926).

8. H. R. Blackwell, and G. A. Bixel, "The Visibility of Non-Uniform Target-Background Complexes: I Preliminary Experiments," Institute for Research in Vision, The Ohio State University Research Foundation Tech. Report No. 890-1 (1960).

APPENDIX A

NORMALIZED PROJECTED SHADOW AREA VERSUS SUN ELEVATION ANGLE AT VARIOUS AZIMUTHS

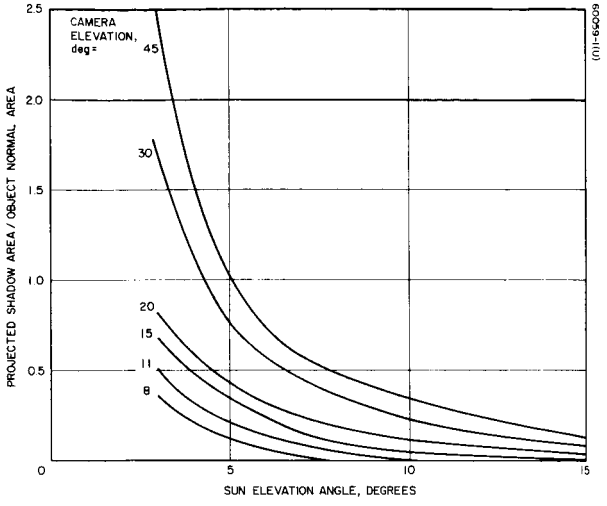

a) 0 Degrees Azimuth

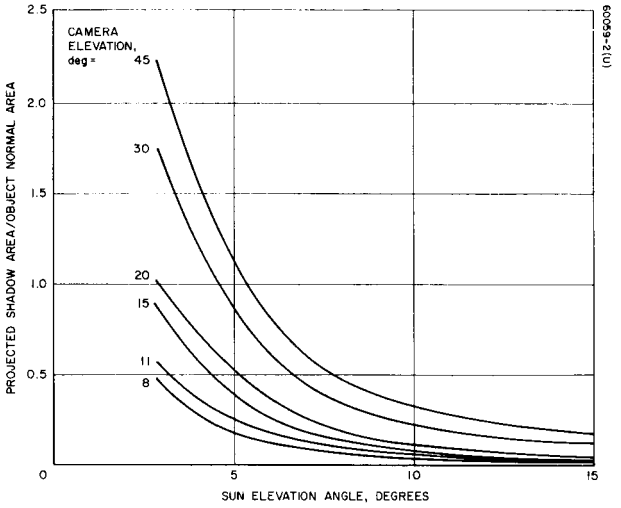

b) 30 Degrees Azimuth

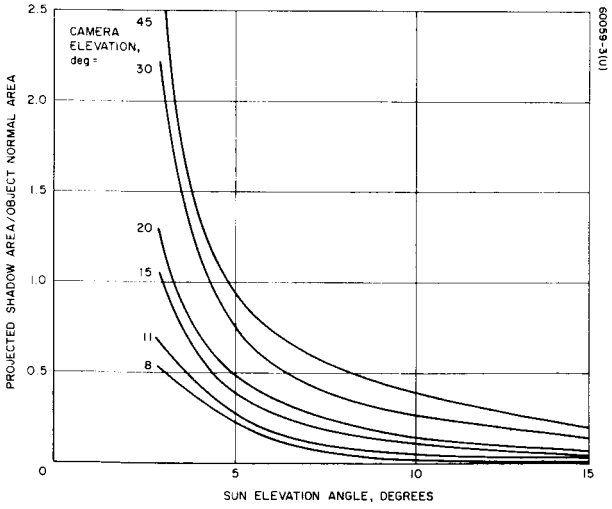

c) 60 Degrees Azimuth

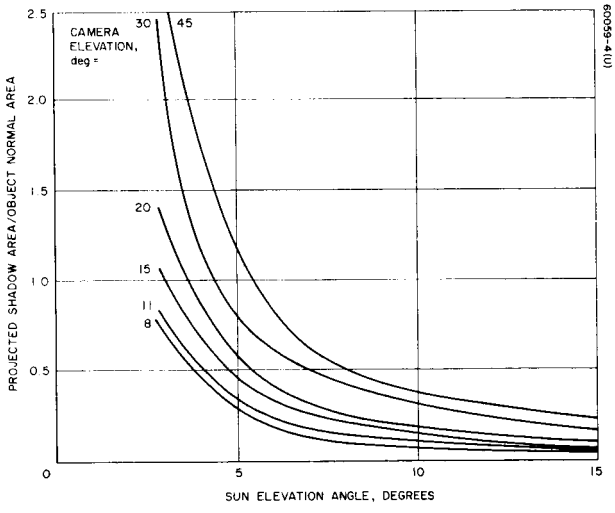

d) 90 Degrees Azimuth

Figure A-1. Convex Spherical Segment

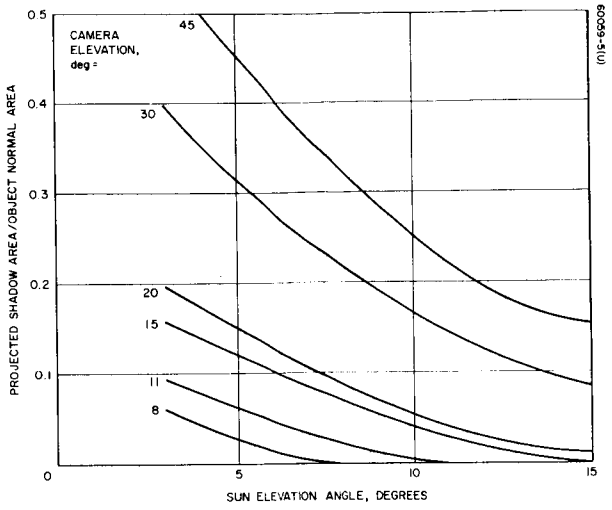

a) 0 Degrees Azimuth

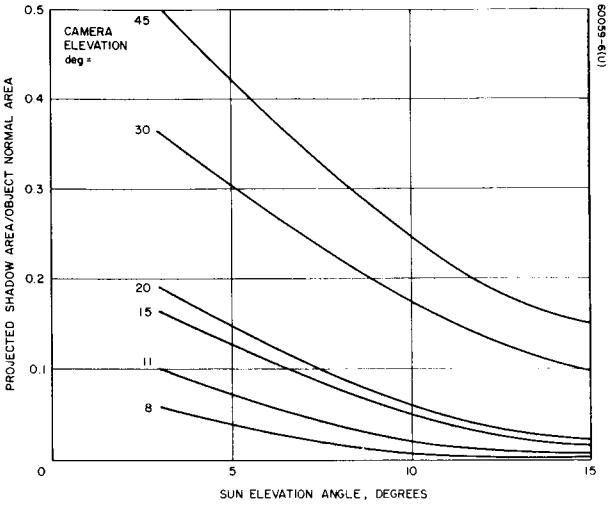

b) 30 Degrees Azimuth

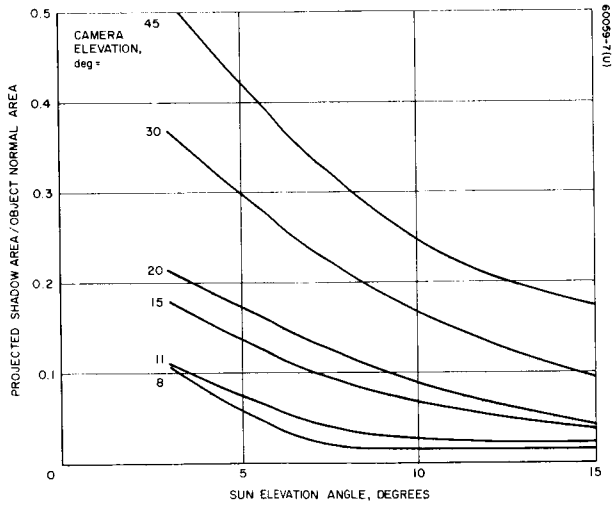

c) 60 Degrees Azimuth

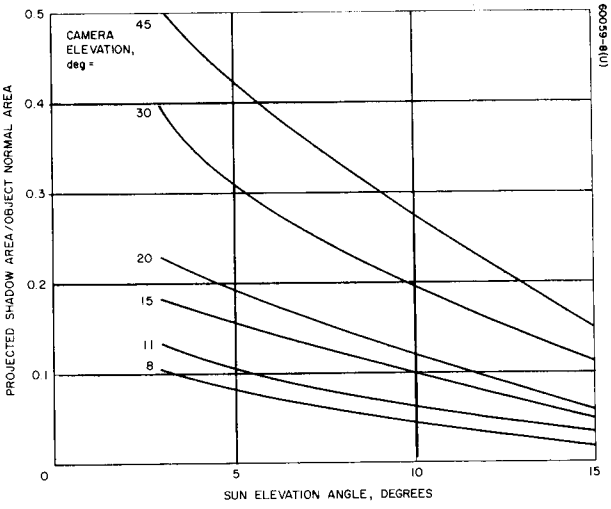

d) 90 Degrees Azimuth

Figure A-2. Concave Spherical Segment

APPENDIX B. PHOTOGRAPHIC TECHNIQUE FOR IMAGERY DEVELOPMENT

The photographic technique developed for solving the imagery problem can be best explained by describing steps in sequential order as actually occuring in the imagery development. These steps are illustrated in Figure B-1 and explained in the following paragraphs.

Step I. Expose the Tri-X-Pan* negative vilms to the CuO_2 dusted wedges which are illuminated by a Xenon light of about one-twelfth solar intensity, at 1/125 second camera shutter speed and five (5) 'f' numbers of 2.8, 4, 5.6, 8, and 11. The exposed negatives are then developed by the Versamat film process machine at the four (4) speeds of 3, 5, 8, and 15 feet per minute with a fixed developer chemical concentration and a constant temperature of 80° F. The CuO_2 dusted wedges used in this step cover the dynamic range of the brightness value of the obstacle detection model. The combinations of the camera lens 'f' number and Versamat speed chosen for negative film development permit a large spectrum of the exposure value. The developed negatives at these combinations of the physical parameters, are then measured by a diffuse densitometer. The measured quantity of the diffuse transmission, T_d, are plotted against the brightness value, E, of the CuO_2 dusted wedges as illustrated in Figure B-2. Twenty (20) entry tables are constructed from these curves for the computer program.**

Step II. Scale Factor Controller - Controls the light intensity during the process of exposing the negative film on the positive by controlling exposure time. The slope 'K' shown in Figure B-1 is the control parameter. In this case, a slope of unity was used throughout the process for simplicity.

---

* Tri-X-Pan was selected because of its fast speed to minimize effects of the film reciprocity.

** The computer program performs the function of the table readout and multiplication.

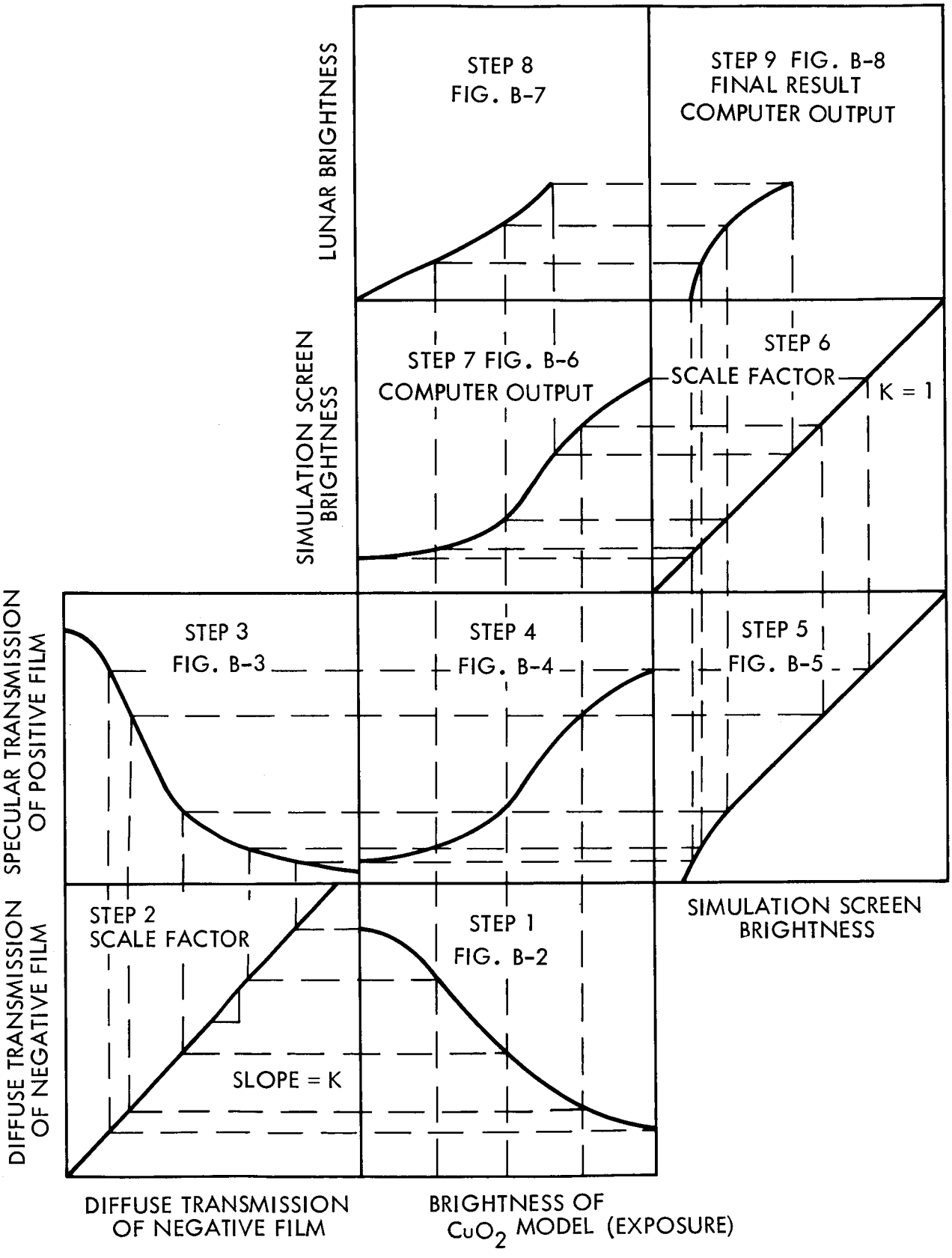

Figure B-1. Sequential Steps of the Photographic Process Technique

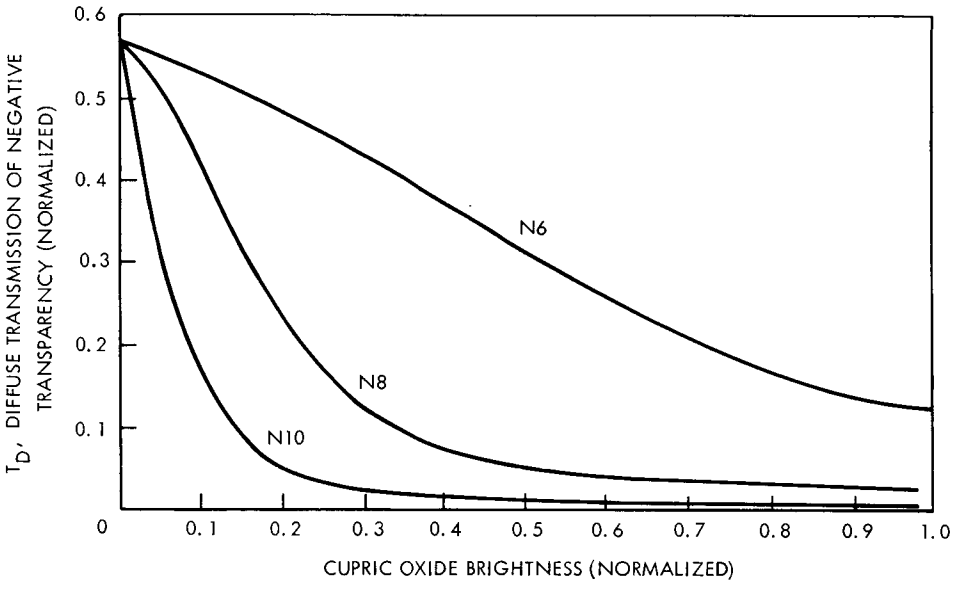

Figure B-2. Photometric Relationship Between Negative Transparency and Cupric Oxide Brightness

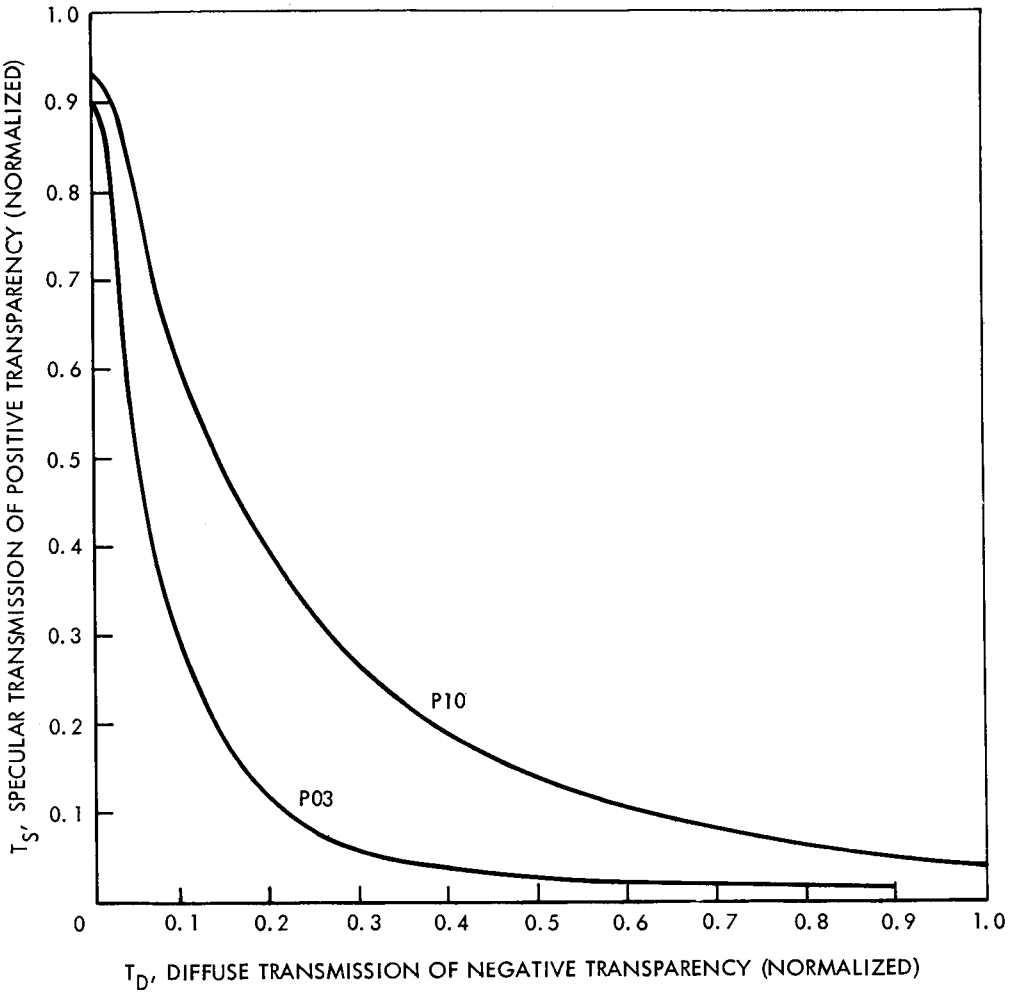

Figure B-3. Photometric Relationship Between Negative Transparency and Positive Transparency

Step III. The exposed positives* are developed using ten (10) Versamat speeds of 2 through 20 feet per minute in two (2) feet per minute increments. We took advantage of the large amount of the information about the specular transmission, T_s, of the Kodak 8430 positive vs. diffuse transmission, T_d, for the above range of Versamat speeds, available in Hughes and used it as an input to the computer program for its multiplication with the curves generated in Step I. Two typical curves of T_s vs. T_d are shown in Figure B-3.

Step IV. By combining the inputs of Steps I and III, the computer generated 200 curves which correlated the values of the CuO_2 dusted wedges and the specular transmission of the positive films. These 200 curves, six of which are shown in Fibure B-4, reenter the computer program as an input to be used in Step V.

Step V. The effects of the projection system and the simulation screen on the brightness values of the positive transparencies are now considered. Measurements of a set of calibrated wedges were used to derive the data graphed in Figure B-5. Twenty individual neutral density wedges selected from a Kodak standard step wedge series were mounted in individual slides and their specular transmission values determined by microphotometer measurement. The effects of the projection system and screen were determined by brightness measurements employing a Spectra brightness meter with 1/2 degree field of view mounted at a distance of 3 feet from the viewing screen. For these measurements a visual surround approximating the size and brightness values employed for the experimental test series was utilized to include wall reflection and stray light effects on screen brightness values.

These curves shown in Figure B-5 correlate the transmission value of the positives (i.e. calibrated wedges) and the brightness values on the simulation screen. They were programmed into the computer for Step VII.

Step VI. Scale Factor Controller - This step, serves only to transform the simulation screen brightness value from abscissa to ordinate in curve plot.

Step VII. The 200 curves developed in Step IV are combined with the single curve of Step V to generate the functional

*Kodak 8430 film was used.

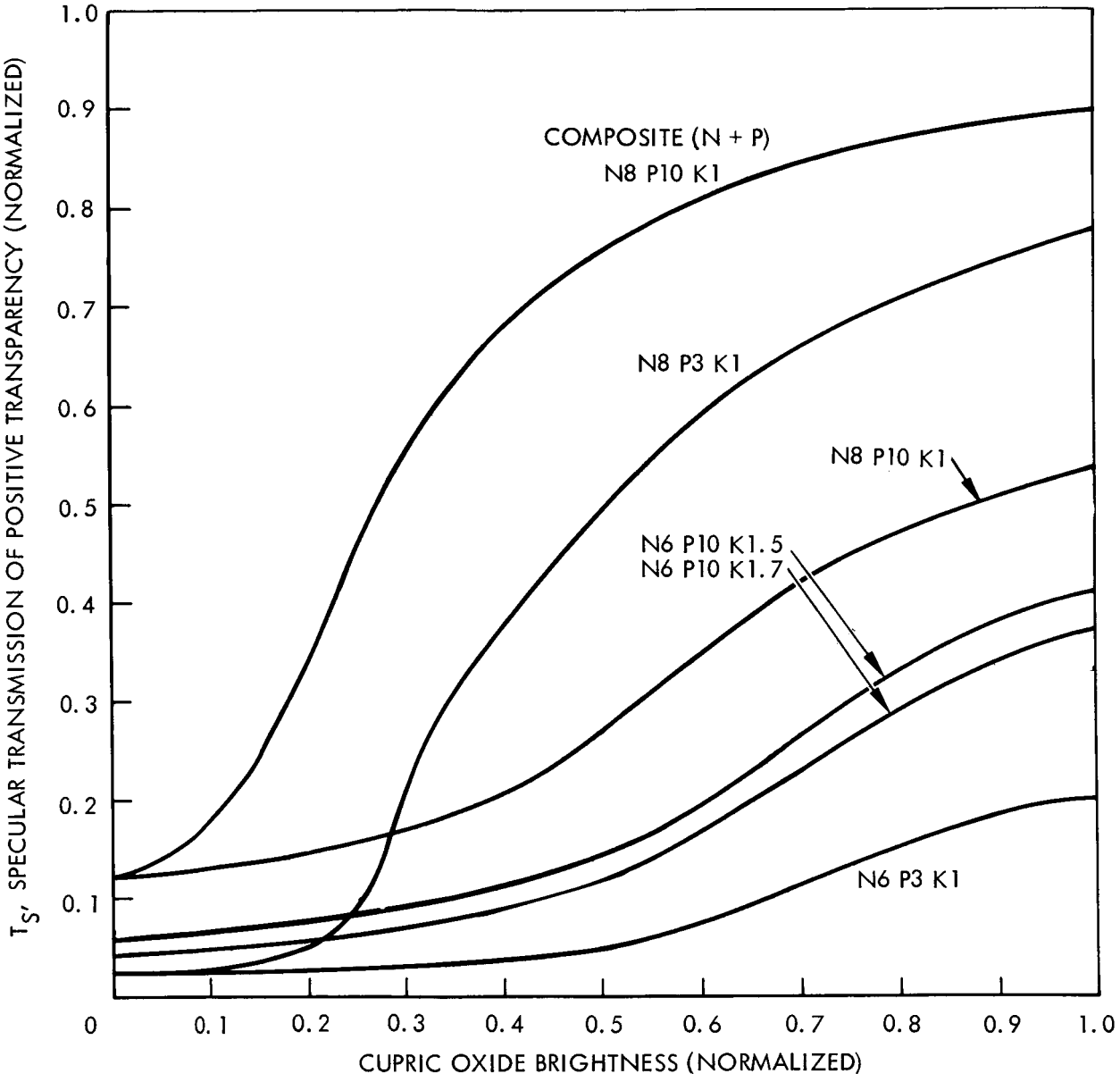

Figure B-4. Photometric Relationship Between Positive Transparency and Cupric Oxide Brightness

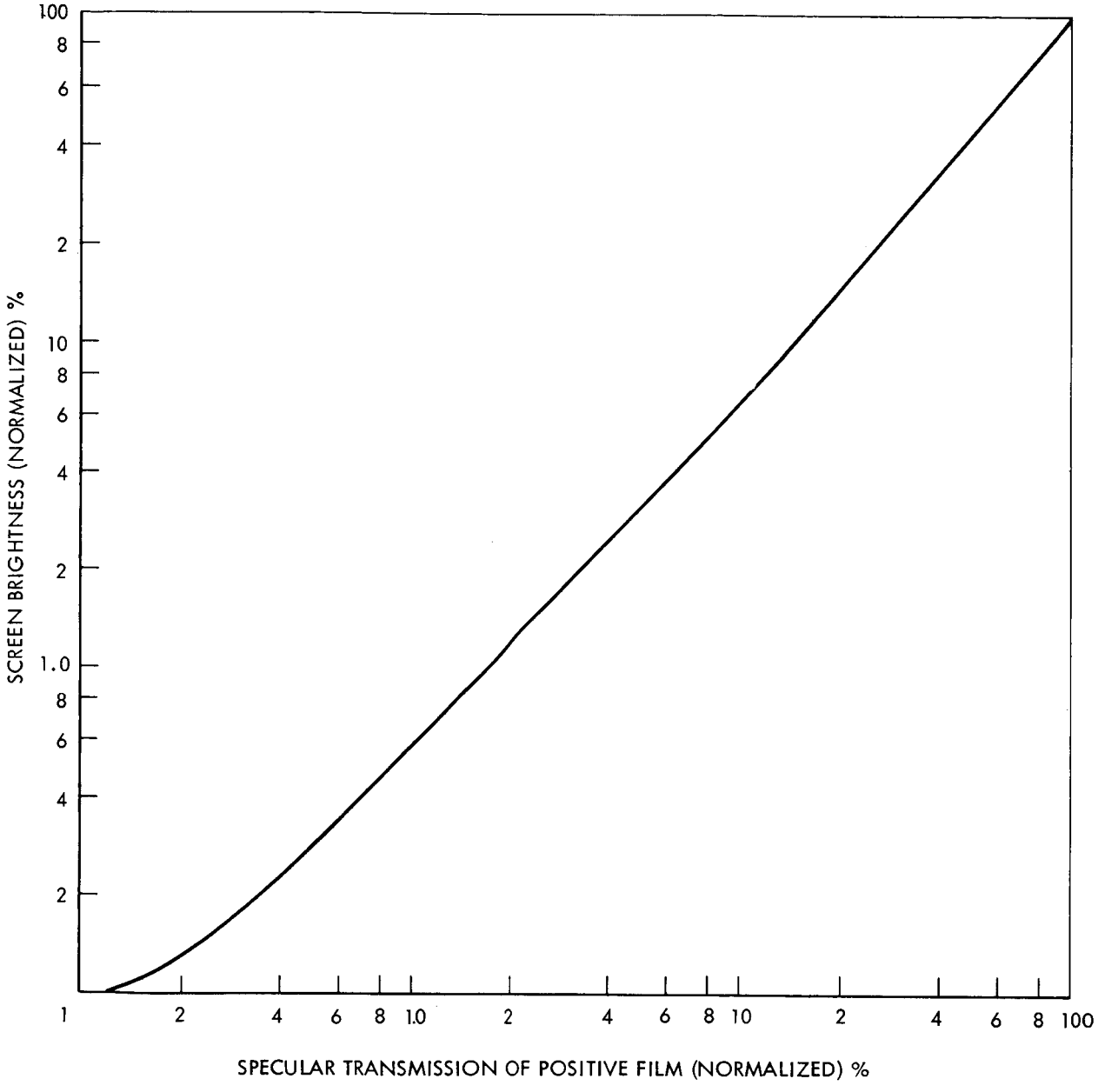

Figure B-5. Screen Brightness versus Specular Transmissibility of Positive Film

relationship between the simulation screen brightness and the brightness of the CuO_2 dusted wedge. Again, 200 curves were generated by the computer, of which 50 were selected for further use. The remaining were discarded as they exhibited very non-linear behavior in the dynamic range in which we are interested. Typical curves obtained from the computer in this step are shown in Figure B-6.

Step VIII. In this step, the brightness value of the CuO_2 dusted wedge furnished by NASA/MSC is plotted against the lunar brightness value based on the J.P.L. photometric function for the twelve simulation conditions tabulated in Figure B-7. The incorporation of these photometric function curves in the imagery development creates a unique feature, wherein the experimental results of the obstacle detection range obtained on the simulation tests can now be directly applied for the conditions which may prevail on the lunar surface.

Step IX. The fifty (50) curves selected in Step VII and twelve (12) curves of Step VIII are entered into the computer program where 600 curves bearing the relationship of the simulation screen brightness values, E, and the lunar brightness values, LB, based on the J.P.L. photometric function, are generated. Sample curves are shown in Figure B-8. In this figure, curves L2 and L6 have been chosen for imagery development based on the selection criteria which is explained in the following paragraph. Each curve can be correlated to specific viewing conditions and photometric parameters used in imagery development. For example, tracing back the steps for curve L2, shows it to correspond to a 5^{o} sun elevation angle, 30^{o} sun azimuth and 14.4^{o} viewing angle, and that control parameters were a 'f' number number of 4.0, Versamat speed of 15 ft/minute for negative development, and 10 ft/minute for positive development.

Criteria for Selection of Curves LB vs. E in Step IX (Lunar Brightness vs. Simulation Screen Brightness).

The 600 curves generated by the computer in the Step IX were carefully examined with respect to the discrepancy in contrast between LB and E. As an example, reference is made to the 6 curves in Figure B-8. Inspection of the curve L2 indicated the bright side-to-background contrast ratio within the dynamic range of the lunar brightness value to be about (.292 - .163)/.163 = .791.

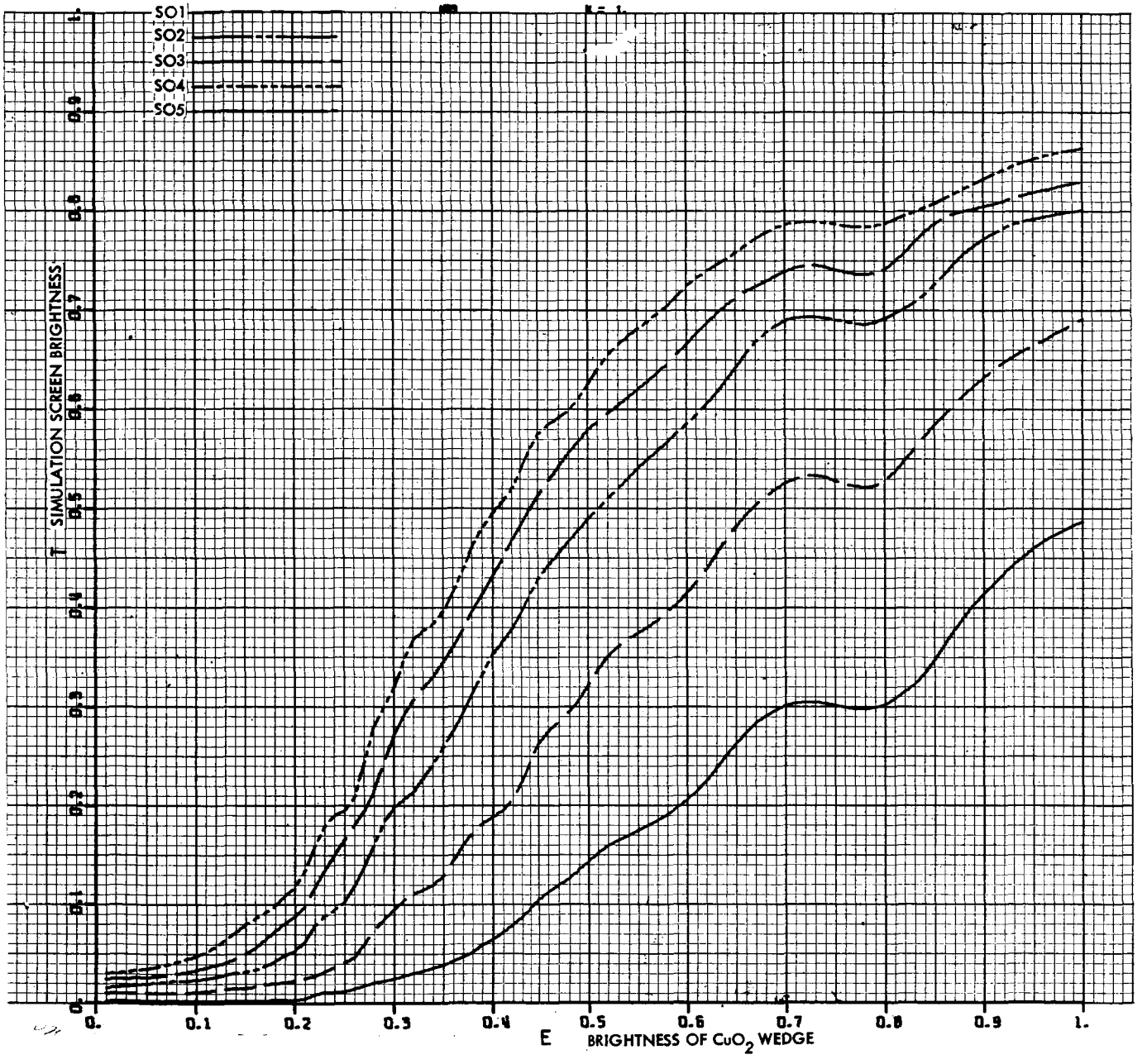

Figure B-6. Simulation Screen Brightness versus Brightness of CuO_2 Wedge

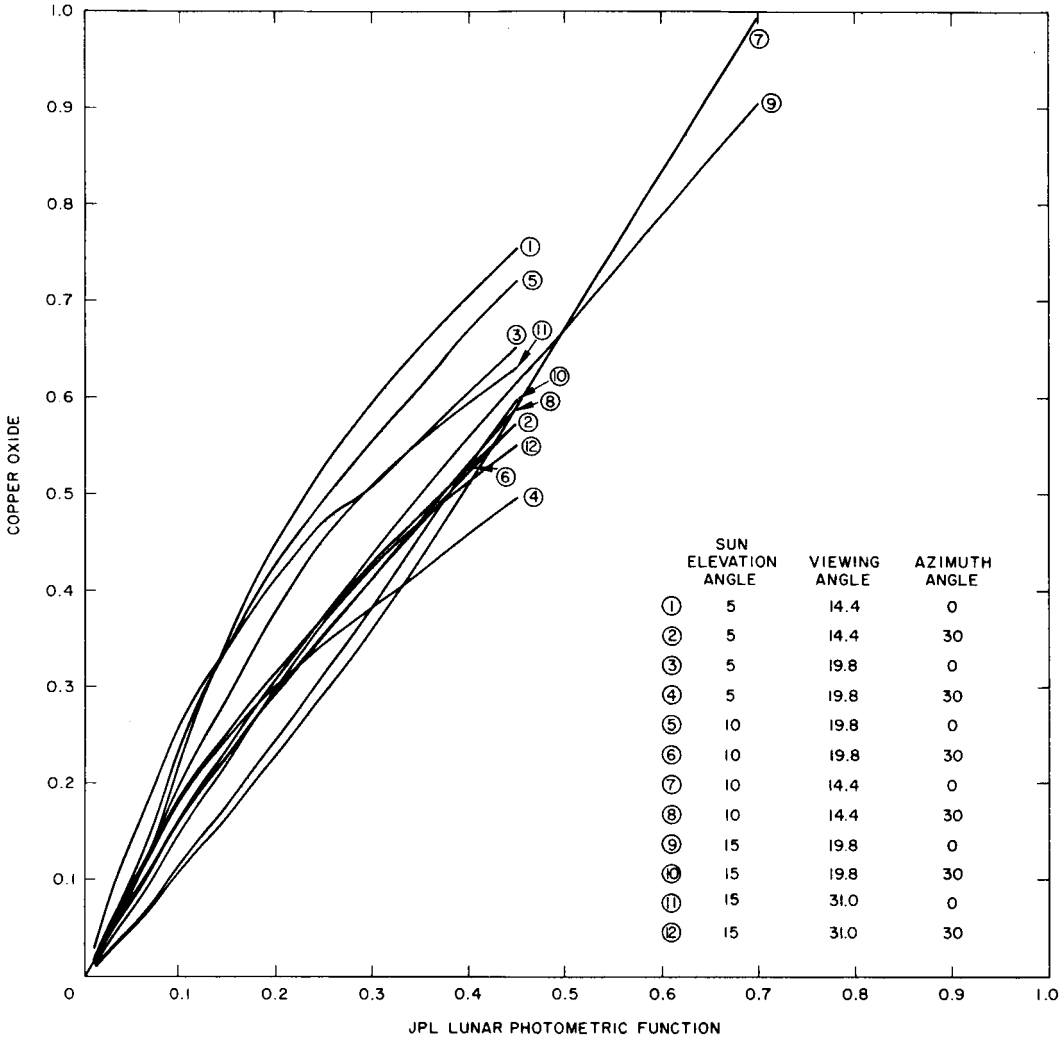

Figure B-7. Brightness Relationship Between Copper Oxide and JPL Lunar Photometric Function for Various Viewing Geometries and Sun Angles

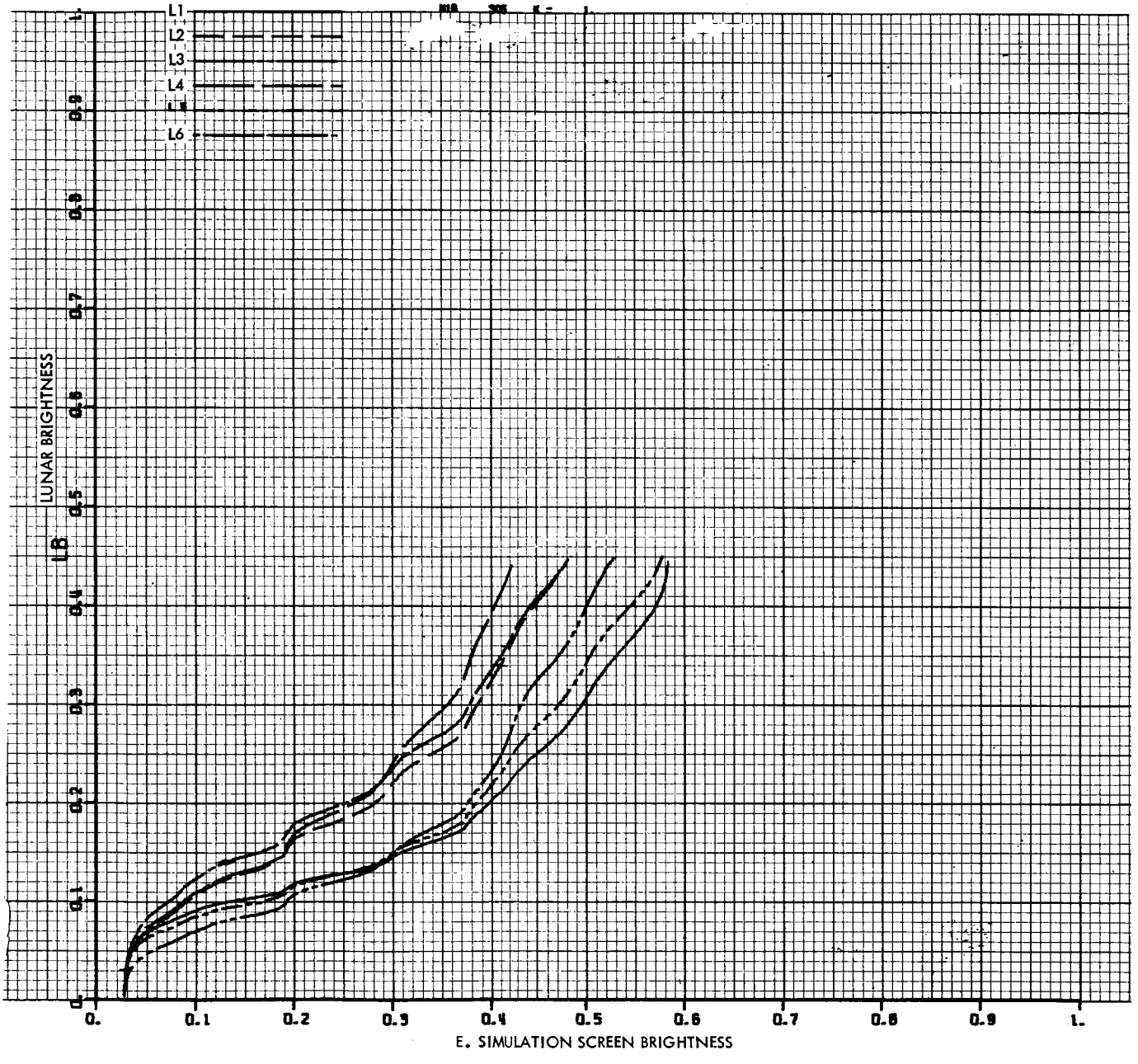

Figure B-8. Final Results of the Computer Output - Lunar Brightness Based on JPL Photometric Function versus Simulation Screen Brightness of Projected Imagery

The corresponding contrast in the simulation screen was (.38-.20)/.20 = .90 for a deviation of approximately 10.9%. The shadow-to-background contrast on the screen will not be equal to unity since the value of E does not vanish at LB = 0. Instead it will be for the worst case (.2-.029)/0.2 = .171/.200=.855 which is about 14.5% error. The uncertainties in both bright side-to-background contrast and shadow-to-background contrast of this curve L2 appeared relatively low as compared with those for other curves. Therefore, it was selected for development of this particular imagery piece.

Sample Piece of Developed Imagery

Three sample pieces of the developed photographic imagery are shown in Figures 5-7, 5-8, and 5-9.